Title

Photodegradation and Heterogeneous OH Oxidation Kinetics and Product Analysis of Aerosolized Triclosan Mixed with NaCl and Humic Acid

Author

Tan, Jong Wen

Publication Date

2022

Peer reviewed|Thesis/dissertation

UNIVERSITY OF CALIFORNIA SAN DIEGO

Photodegradation and Heterogeneous OH Oxidation Kinetics and Product Analysis of Aerosolized Triclosan Mixed with NaCl and Humic Acid

A Thesis submitted in partial satisfaction of the requirements
for the degree Master of Science

in

Chemistry

by

Jong Wen Tan

Committee in charge:

Professor Jonathan Hall Slade, Chair
Professor Lihini Indira Aluwihare
Professor Robert S Pomeroy

2022

The Thesis of Jong Wen Tan is approved, and it is acceptable in quality and form for publication on microfilm and electronically.

University of California San Diego

2022

DEDICATION

To my family.

TABLE OF CONTENTS

LIST OF FIGURES

LIST OF TABLES

LIST OF ABBREVIATIONS

2,4 DCP	2,4 dichlorophenol
2,8 DCDD	2,8 dichlorodibenzo-*p*-dioxin
4-CC	4-chlorocatechol
CDOM	Chromophoric dissolved organic matter
DMA	Differential mobility analyzer
EESI-HR-ToF-MS	Extractive electrospray ionization high resolution time-of-flight mass spectrometry
HA	Humic acid
NaCl	Sodium chloride
OH	Hydroxyl radical
PAM-OFR	Potential aerosol mass oxidation flow reactor
SEMS	Scanning electrical mobility spectrometer
SSA	Sea spray aerosol
TCS	Triclosan

ACKNOWLEDGEMENTS

First and foremost, I would like to thank Professor Nate Slade for his guidance and patience as an advisor and an exceptional scientist. He constantly inspires me with his knowledge and passion for research and taught me the importance of seeing the bigger picture. Under his guidance, I gained valuable research experience and the life skills of building resilience and confidence. I am forever grateful for the opportunity to conduct research in Professor Nate Slade's lab.

I would also like to thank my committee members Professor Aluwihare and Professor Pomeroy for helping me advance my graduate education. In particular, working as a teaching assistant for Professor Pomeroy had been a greatly rewarding experience as I learned how to be a teacher from him.

I am most grateful for all the members of the Slade group, including Benjamin Carr, Adam Cooper, Allison Kawasaki, Samantha Kruse, Karen Lopo-Zepeda, Lincoln Mehndiratta, Renee Niles, and Ryan Tumminello, for their support and guidance. Especially, I would like to thank Samantha Kruse for being my mentor as I joined the lab as an undergraduate and continuing to serve as a mentor throughout my graduate career. She trained me on all the instrumentation, guided me through my experimental setup and analysis, and answered every little or big question I had. Completion of this thesis would not have been possible without the support of the Slade group.

Last, but not least, I want to thank my family and friends. Thank you to my mom and dad for always supporting me in exploring my passion and decisions in life. Thank you to my brother who is always there checking in on me. Thank you to my grandma for your unconditional love.

Chapters 1 through 4, in part, coauthored with Slade, Jonathan H., is currently being prepared for submission for publication under the title, “Photodegradation and heterogeneous OH oxidation kinetics and products of triclosan in sea spray aerosol mimics.” The thesis author is the primary author of these chapters.

ABSTRACT OF THE THESIS

Photodegradation and Heterogeneous OH Oxidation Kinetics and Product Analysis of Aerosolized Triclosan Mixed with NaCl and Humic Acid

by

Jong Wen Tan

Master of Science in Chemistry

University of California San Diego, 2022

Professor Jonathan Hall Slade, Chair

Triclosan, an antimicrobial agent incorporated in personal care and consumer products, is used to prevent bacterial contamination and material biodegradation. However, various studies have shown that triclosan exhibits toxic effects to aquatic species, persists in the environment, and poses as an endocrine disruptor. Triclosan can be leached from untreated wastewater and wastewater treatment plant effluent into ocean surface water as a contaminant. Consequently, it

can become aerosolized in sea spray aerosol (SSA) and undergo degradation in the atmosphere to produce potentially more toxic transformation products, such as dichlorodibenzo-*p*-dioxin and chlorophenols. To understand the lifetime of triclosan in the aerosol phase in SSA, this research focuses on quantifying the kinetics and degradation lifetimes of triclosan with respect to heterogeneous oxidation by hydroxyl radicals (OH) and photosensitization reactions involving chromophoric dissolved organic matter (CDOM) mixed with inorganic salts that coexist in SSA. A potential aerosol mass oxidation flow reactor (PAM-OFR), used to simulate aerosol aging, is coupled with an extractive electrospray ionization high-resolution time-of-flight mass spectrometer (EESI-HR-ToF-MS) to study triclosan degradation kinetics and its transformation products in the aerosol phase in near real time. Results indicate that the reactive uptake of OH by single-component triclosan aerosol proceeds with a diffusion-corrected uptake coefficient of 0.15 ± 0.04. In the presence of humic acid, a CDOM proxy, the OH reactive uptake coefficient decreased to 0.09 ± 0.04, suggesting that CDOM inhibits triclosan degradation in the presence of OH radicals. Furthermore, the addition of the inorganic salt, NaCl, to the triclosan system increased the effective uptake coefficient to 0.29 ± 0.08. 2,8 dichlorodibenzo-*p*-dioxin (2,8 DCDD), a toxic transformation product, was potentially detected by the EESI-HR-ToF-MS in the aerosol phase indicating photodegradation as the major degradation pathway of triclosan. The half-life of triclosan in the aerosol phase with respect to heterogeneous oxidation by OH is estimated to be 18.63 ± 4.53 days. This project aims to gain a better understanding of the effects of photodegradation and OH radical heterogeneous oxidation on the lifetime of triclosan in the aerosol phase, the influence of added photosensitizer and inorganic salt, and potentially the contribution of triclosan degradation to the formation of more toxic transformation products.

Chapter One: Introduction

1.1 Triclosan and Its Associated Health and Environmental Impacts

Triclosan (TCS), an antimicrobial ingredient, is found ubiquitously in our environment (see Fig. 1). It is incorporated into a broad range of consumer and commercial products including textile, toys, toothpaste, and hand sanitizers, to prevent material degradation and hinder bacterial growth[1–4]. More commonly, triclosan is found as an active ingredient in personal care products[5]. Since its discovery in the 1960s, there has been an estimated global triclosan production of 1,500 tons per year in 1998 and an estimated 4,762 tons manufactured in 2015[1,2,6–11]. Field studies conducted regarding the presence of triclosan in the environment have detected varying concentrations in surface water, wastewater influent and effluent, seawater, soil, sewage sludge, indoor dust, and even food and drinking tap water (see Fig. 2)[8,12–16]. Its prevalence has sparked further investigations to evaluate the potential health risks and environmental effects due to the exposure to and accumulation of this antimicrobial agent.

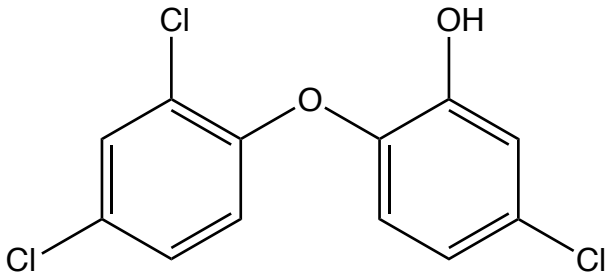

Figure 1. Structure of Triclosan (5-chloro-2-(2,4-dichlorophenoxy)phenol).

In vivo and *in vitro* studies have shown that triclosan can accumulate in the human body[10]. Ingestion and epidermal permeation are the common routes of human exposure to

triclosan[11,12,15,17]. Through different levels of exposure, varying concentrations of triclosan were detected in human breastmilk, urine, and hair samples[10,12]. Gonkowski et al. 2022 found triclosan in 96.7% of the human hair sampled from residents of Olsztyn, Poland[12]. Van der Meer et al. 2017 detected triclosan in the hypothalamus of post-mortem brain analysis revealing the ability of this antimicrobial to infiltrate the brain, which sparks further needs to research its potential influence on metabolic regulations[18]. Categorized as an endocrine disruptor by the National Institute of Environmental Health Sciences, triclosan also has the potential to pose serious reproductive health effects[19]. Wang et al. 2015 reported the first *in vivo* study that highlighted the potential for triclosan exposure to cause spontaneous abortions in humans and mice as they found the detectable rate of triclosan in patients who experienced spontaneous abortions to be 1.76 times higher than in normal pregnancy patients[20]. The multitude of studies points to the need to regulate triclosan usage to mitigate the associated adverse health effects.

Various studies have highlighted the environmental persistence and bioaccumulation of triclosan[1,10,11]. As an antimicrobial found in personal care products, triclosan is primarily disposed of down residential drains[21]. During wastewater treatment processes, the majority of triclosan present either biodegrades or gets absorbed to active sludge that in turn is used as biosolid for agricultural purposes[22]. With a relatively high log K_{ow} value of 4.8, triclosan exhibits high absorption to solids[2,23,24]. Bock et al. 2010 found an estimated 30 - 52% removal of triclosan from wastewater to active sludge[5,25]. Barrett et al. 2022 also measured triclosan to be the predominant antibacterial monitored in sewage sludge from Ontario, Canada[26]. Despite studies showing high rates of triclosan removal from wastewater treatment plants (WWTP), ranging from 58 - 95%, the remaining fraction will enter surface waters as a contaminant[21,27]. The worldwide triclosan concentration was measured to range from 23 - 5,370 ng/L in

wastewater effluent, 1- 40,000 ng/L in surface water (lake/river), and <100 ng/L in sea water[1]. In particular, a study that measured triclosan concentration in wastewater treatment plant effluent samples from Durban metropolis in South Africa found triclosan concentration ranging as high as from 1.732 - 6.980 µg/L[22]. The variance in triclosan concentration in different water matrices can be attributed to disparities in corresponding population density, regulations, and the efficiency of triclosan and other contaminant removal at specific WWTPs[27].

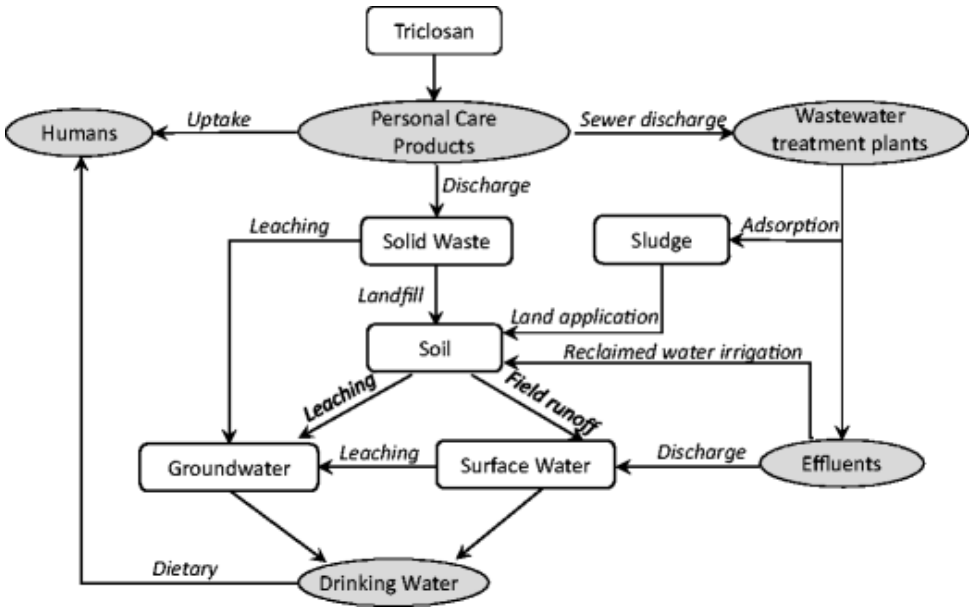

Figure 2. Schematic highlighting the potential pathways for triclosan exposure. Image from Chen et al. 2018[16].

Once in the environment, triclosan, a hydrolytically stable and lipophilic antimicrobial, can be readily taken up by aquatic organisms[7,10,23,28,29]. To understand the ecotoxicity effects of triclosan, studies on animal exposure to high levels of triclosan were conducted. Results indicated that aquatic organisms exhibit reproductive disruptions and developmental deformities under high triclosan exposure[1,30,31]. Hwang et al. 2014 found a significant decrease in sea urchin sperm viability and embryonic development after exposure to 1µM of triclosan and above[30]. Zhang et al. 2018 also found that high exposure to triclosan led to malformation and eye cell

death in zebrafish[31]. Additionally, various studies explored the potential for triclosan to induce antibiotic resistance in bacteria. Westfall et al. 2019 found exposure to environmentally relevant concentrations of triclosan increased *E. coli* and methicillin-resistant *Staphylococcus aureus* (MRSA) antibiotic tolerance up to 10,000-fold in an *in vitro* study[32]. The abundant evidence on the ubiquity, adverse health effects, environmental persistence, and ecotoxicity of triclosan point to the need to understand the presence and chemical lifetime of triclosan in our environment.

Regulations on triclosan in personal care and consumer products vary globally. The health and environmental concerns regarding triclosan, in conjunction with the lack of research evidence to prove the effectiveness of triclosan addition in antimicrobial soaps, motivated the FDA announcement in 2016 to ban all over-the-counter soaps containing triclosan along with 18 other active ingredients[33]. Despite the ban on triclosan usage in over-the-counter soaps in the U.S., it is still prevalent in other products not regulated by the FDA and in other countries[1]. In Canada, triclosan is allowed to be incorporated at a concentration up to 1% in non-prescription drugs and the European Commission allows a maximum concentration of up to 0.3% in cosmetic products[34,35]. In other countries, the use of triclosan is not regulated. Chen et al. 2018 detected triclosan in 95% of the 283 urine samples from children in South China with a median concentration of 0.21 μg/L[36].

In addition to the host of adverse effects associated with triclosan exposure, it can also undergo photodegradation to generate more toxic transformation products, including 2,8 dichlorodibenzo-*p*-dioxin (2,8 DCDD) and 2,4-dichlorophenol (2,4-DCP)[24,37]. As shown in Fig. 3, triclosan present at a higher pH absorbs electromagnetic radiation in a range that overlaps with the solar spectrum, which reveals its ability to photodegrade in the natural environment[24]. The degradation kinetics of triclosan in water was observed to vary depending on the environmental

conditions, such as pH value, wavelength of light exposure, and the presence of other potential photosensitizing species[1,37]. 2,8 DCDD, known as a polychlorinated dibenzo-*p*-dioxin formed from the photocyclization of triclosan, is listed in the Stockholm Convention as a persistent organic pollutant[37–40]. Another major triclosan photoproduct, 2,4-dichlorophenol, is formed from triclosan ether bond cleavage[39]. To explore the health-related concerns of 2,4-DCP, an *in vitro* study by Bukowska et al. 2016 found that exposure to high concentrations of 2,4-DCP leads to increased reactive oxygen species (ROS) formation in human peripheral blood mononuclear cells which induces cell oxidative stress[41]. Once triclosan enters coastal waters from wastewater effluents, mechanical processes such as breaking waves and bubble rupturing at the water's surface (e.g. as in coastal marine environments and in large freshwater bodies including the Great Lakes) are expected to loft triclosan into the air in the form of sea spray aerosols. Subsequent reactions via degradation through photochemical and heterogeneous reactions with trace gaseous species in the atmosphere may lead to the formation of more toxic oxidation and photoproducts that are respirable in aerosol. The prevalence of triclosan in the environment, its proven toxicity to ecosystems, its associated toxic phototransformation products, and its hazard to human health warrant further studies and stricter regulations to understand its chemical lifetime in the environment and to control the output of this pollutant.

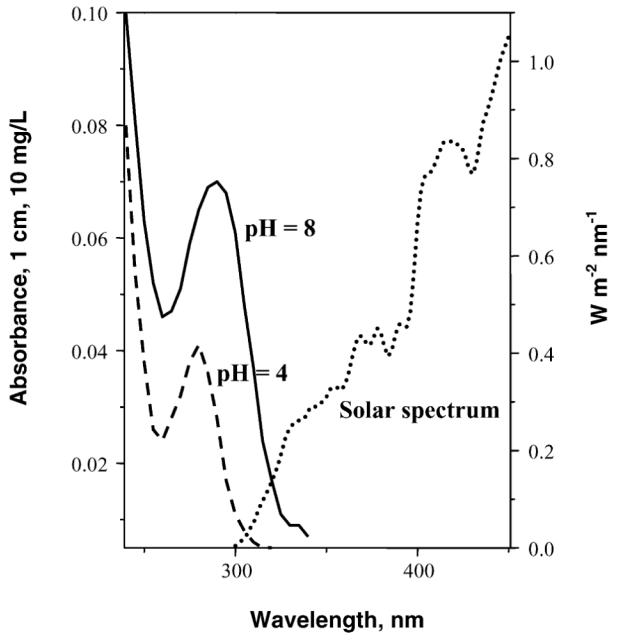

Figure 3. Absorbance spectrum for triclosan at two different pH values compared to the solar spectrum. Image from Mezcua et al. 2004[24].

1.2 Sea Spray Aerosol Formation: Influence of Photosensitizers and Inorganic Salts

Sea spray aerosol (SSA), formed from bubbles bursting in the sea surface microlayer, contributes to a large fraction by mass of the particulate matter in the atmosphere[42–44]. SSA is comprised of inorganic salts and organic matter[43,45]. Since SSA reactivity, chemical lifetime, and transport are largely dictated by its chemical composition, it is imperative to understand how the presence of inorganic salts and dissolved organic matter (DOM) can influence characteristics of SSA[44,45].

A pathway for particle chemical transformation in the environment is through photochemical reactions. Photochemistry can take the form of direct photolysis, which is where the particles are transformed through absorption of sunlight, and indirect photochemistry, which occurs when natural photosensitizers absorb sunlight and produce reactive transient species that

react in the particle phase with neighboring species[46,47]. Specifically in aquatic environments, the presence of DOM has been found to induce indirect photochemical reactions[48]. The fraction of DOM that absorbs sunlight in the marine environment is classified as marine chromophoric dissolved organic matter (m-CDOM)[47]. It can act as a photosensitizer after light absorption to generate reactive species including OH radicals, excited state oxygen, and the excited triplet state of the photosensitizer[49]. A large fraction of CDOM is composed of humic substances[50]. Therefore, this study evaluates the effects of using humic acid as a proxy for m-CDOM to understand the photosensitizer effects on triclosan aerosol degradation.

The distribution of organic matter to inorganic salts in SSA composition is important for the size determination of the particles[45,51,52]. The presence of inorganic salt can affect the surface tension and water density which influences the bubble bursting mechanism in SSA formation[52]. Additionally, studies have shown that increases in ionic strength of DOM-containing solutions correspond to an increase in photoabsorbance of DOM[53,54]. Therefore, understanding how the presence of salt ions affects photochemical processes of aerosolized particles is important in elucidating the reactivity of the particles. With sodium and chloride ions accounting for the largest fraction of ions present in seawater, NaCl can serve as an important proxy for the influence of ionic strength on SSA reactivity.

1.3 Multiphase Oxidation Kinetics and Hydroxyl Radical Formation

Suspended aerosol particles can undergo multiphase oxidation reactions with reactive trace gases present in the atmosphere, which may further influence the particles' reactivity, toxicity, or lifetime. Atmospherically relevant reactive trace gases include ozone (O_3), hydroxyl radicals (OH), and nitrate radicals (NO_3)[55]. Of the oxidizing gases, hydroxyl radical is considered

to be the most important oxidant in the troposphere and is referred to as the "detergent of the atmosphere"[55–57]. Due to the high reactivity of hydroxyl radicals with an atmospheric lifetime of around one second, they are effective at removing air pollutants, such as carbon monoxide (CO), methane (CH_4), and hydrochlorofluorocarbons (HCFCs) from the atmosphere[56]. Therefore, hydroxyl radicals serve as an important sink for such pollutant gases[58,59].

The primary formation pathway for hydroxyl radicals in the troposphere is through a series of reactions involving the breakdown of ozone by UV radiation to produce excited oxygen atoms that then react with water vapor (see Eq. 1 and Eq. 2)[58,60]. Subsequent to oxidation of pollutant gases, OH is regenerated and recycled back into the system, which helps maintain the relatively constant overall concentration of OH in the atmosphere[56,58].

$$O_3 \xrightarrow{h\nu\ (\lambda < 330nm)} O_2 + O(^1D) \qquad \textit{Eq. 1}$$

$$O(^1D) + H_2O \rightarrow 2OH \qquad \textit{Eq. 2}$$

Another important source of hydroxyl radicals in urban regions is the photolysis of nitrous acid (HONO) (see Eq. 3)[61,62]. There has been a number of pathways identified for HONO production in the atmosphere, some include direct emissions from fossil fuel combustion, hydrolysis of NO_2, and reaction of NO and OH radicals[61,63]. In the atmosphere, HONO becomes an important precursor for OH[61]. Kleffmann et al. 2007 found in field measurements that the presence of HONO contributed up to 56% of OH produced[62].

$$HONO \xrightarrow{h\nu\ (\lambda < 390nm)} NO + OH \qquad \textit{Eq. 3}$$

With the presence of OH in the atmosphere, SSA may undergo heterogeneous oxidation through uptake of OH on the particle surface (see Fig. 4)[64]. It is important to study the effects of chemical aging, which is the transformation of aerosols through atmospheric transport, because

aerosol composition and characteristics can be altered, and hence influence their climate effects[65,66]. This study focuses primarily on OH reactive uptake to understand the influence of OH heterogeneous reactions on triclosan's potential chemical lifetime and degradation in the environment.

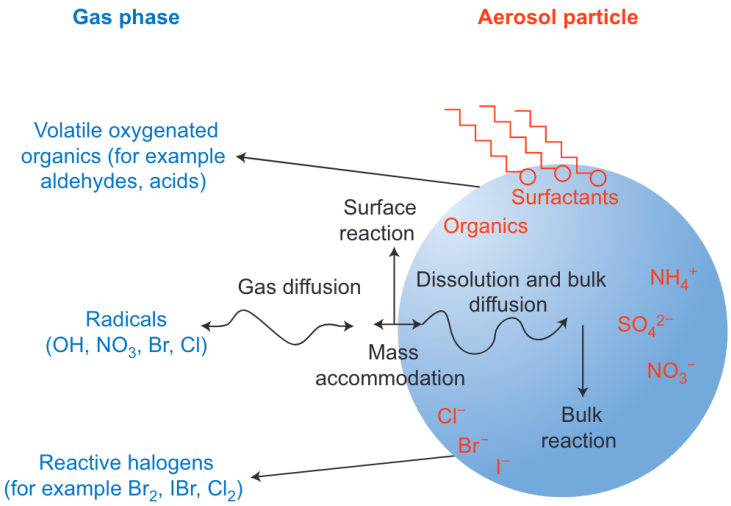

Figure 4. Heterogeneous reactions of gas phase species and aerosol particles. Image from George et al. 2010[97].

1.4 Background on Triclosan Degradation Kinetics and Product Formation

Extensive studies have been conducted to quantify the degradation kinetics of triclosan due to direct and indirect photodegradation in the aqueous phase[38]. The effects of solution pH, water sample medium, and the wavelength of irradiance for photolysis were found to be significant factors that determined triclosan degradation kinetics[1,14].

With a pKa of 7.9-8.2, triclosan can be detected in its molecular form or its dissociated anionic form in natural waters[38,49]. Various studies observed the phenolated, anionic form of triclosan to degrade significantly faster than the molecular form of triclosan under irradiance[24,37,67,68]. Tixier et al. 2002 found that an increase in the light absorption rate of

triclosan was due to the higher degree of overlap between triclosan absorption spectrum in solutions of increasing pH and the solar spectrum (see. Fig. 3)[69]. Despite the significant increase in the rate of triclosan degradation in higher pH solutions, 2,8 DCDD, a triclosan photodegradation product, was still detected in a solution with a pH as low as 3 by Sanchez-Prado et al. 2006[67].

Another parameter that strongly influences triclosan photodegradation kinetics is the presence of photosensitizers in the solution medium[38]. To explore the indirect photodegradation effects of photosensitizers on triclosan, various studies have observed the influence of nitrate (NO_3^-) and humic acid addition to triclosan sample solutions[38,69,70]. Humic acid is incorporated as a proxy for m-CDOM, a main sunlight absorber in natural waters, to explore the effects of photosensitizers in aquatic systems on triclosan degradation[47]. The effects of nitrate, a common ion present in aquatic matrices, as a photosensitizer were also explored in previous studies. However, a consensus on the influence of photosensitizers in triclosan photodegradation has not been established[38]. Iovino et al. 2019 showed that the addition of humic acid to a synthetic solution of triclosan dissolved in water rapidly increased the rate of triclosan removal under irradiance[37]. Iovino et al. 2019 also observed an increase in triclosan degradation with the addition of NO_3^- that they attributed to the influence of OH formation from nitrate photodecompostion[37]. In another study, Latch et al. 2005 suggested, according to their experimental findings, that the increase in triclosan photodegradation in natural water was due to the presence of humic matter[68]. Conversely, Tixier et al. 2002 found that the addition of humic acid led to a 20% decrease in triclosan phototransformation rate[69]. Due to the varying conclusions drawn on the effects of CDOM on triclosan degradation, further research to confirm the photosensitizer effects of CDOM is necessary.

The presence of inorganic salt in sea spray aerosol can also influence the heterogeneous oxidation of triclosan in the aerosol phase. Knipping et al. 2000 observed that the presence of NaCl undergoing heterogeneous reactions with hydroxyl radicals contributes to strong chloride ion interaction with gaseous hydroxyl radicals resulting in chlorine formation[71]. From a triclosan degradation study, Aranami and Readman et al. 2007 attributed the observed enhancement in triclosan photodegradation in wastewater compared to in pure water to the potential contribution of salinity, metal ions, and pH[72]. The presence of inorganic salts could also interfere with the light absorption capacity of CDOM, which could impact its photosensitizing effects[54]. With sodium and chloride ions accounting for 86% of all dissolved chemical species in seawater, the influence they can cast on triclosan phototransformation in sea spray aerosol cannot be ignored[73].

With the ubiquity of triclosan in surface waters and previous identification of toxic transformation product formation from triclosan degradation in solution, it raises important questions regarding the chemical lifetime and product formation potential of triclosan suspended in the atmosphere in sea spray aerosol. Despite the extensive studies conducted on triclosan degradation and the effects of photosensitizer addition, few studies were conducted on the effects of triclosan in the aerosol phase. Therefore, this study aims to provide insight on how the inclusion of humic acid and NaCl influence the heterogeneous oxidation of triclosan in the aerosol phase and the potential formation of transformation products due to triclosan degradation.

Chapter 1, in part, coauthored with Slade, Jonathan H., is currently being prepared for submission under the title, “Photodegradation and heterogeneous OH oxidation kinetics and products of triclosan in sea spray aerosol mimics.” The thesis author is the primary author of this chapter.

1.5 Research Objectives

The goal of this thesis is to understand the photodegradation and heterogeneous oxidation kinetics of triclosan, an antimicrobial, in the aerosol phase. To simulate SSA conditions, the degradation rate constant and OH reactive uptake coefficient of aerosolized triclosan are quantified both in the presence and absence of inorganic salt and a representative photosensitizer. Additionally, the method of using EESI-HR-ToF-MS, an online analytical method, to measure aerosolized triclosan and its transformation products is explored.

This thesis attempts to answer the following scientific questions:

1. Can EESI-HR-ToF-MS be used to characterize aerosol composition of triclosan, a chlorinated pollutant, and its transformation products?
2. How is the lifetime and degradation kinetics of triclosan in the aerosol phase influenced in the presence of light and OH radicals?
3. How does the addition of inorganic salts and photosensitizers, specifically NaCl and humic acid, affect aerosolized triclosan degradation kinetics and chemical lifetime in the presence of OH radicals?

Chapter Two: Experimental

This section details the experimental procedures performed including the chemicals used and the instrumentation employed for quantitative and qualitative analysis of triclosan and its transformation products. Figure 5 shows a schematic of the experimental setup. Triclosan solutions were prepared from triclosan powder (Purity > 97%, Sigma-Aldrich) at a concentration of 200 ppm dissolved in 80% methanol and 20% water. HPLC-grade water and methanol were used as solvents for triclosan solution preparation. Triclosan solutions were aerosolized with an atomizer (Model 3076 TSI Inc.). Subsequently, the aerosolized particles flowed through a diffusion drier (Brechtel Inc.), an aerosol neutralizer (Brechtel Inc.) using Po-210 (NRC), and then a differential mobility analyzer (DMA; Brechtel Inc.) to generate monodisperse particles. Then, triclosan aerosol particles were sampled into a potential aerosol mass oxidation flow reactor (PAM-OFR; Aerodyne) equipped with low-pressure mercury lamps irradiated at a wavelength of 254 nm. Two separate lines of compressed zero air, one through a humidifier and another through an external ozone chamber, were flowed into the PAM-OFR to generate OH via the photolysis of ozone in the presence of water vapor. In the reactor, triclosan aerosol particles were subjected to different concentrations or "exposures" of OH controlled by varying the 254 nm lamp voltage/intensity. From the output, the size of the particles was monitored using a scanning electrical mobility spectrometer (SEMS; Brechtel Inc.), the ozone concentration was measured using an ozone monitor (2B Technologies Inc.), and the output composition was analyzed using an extractive electrospray ionization high-resolution time-of-flight mass spectrometer (EESI-HR-ToF-MS; Aerodyne). Systems with humic acid (HA) and sodium chloride (NaCl) were also studied to mimic the composition of sea spray aerosol. The setup and procedure for them were identical to the one described above except the atomized solutions were

composed of either the addition of humic acid at a concentration of 200 ppm or NaCl at a concentration of 200 ppm, and the last was composed of a mixture of 200 ppm HA and 200 ppm NaCl.

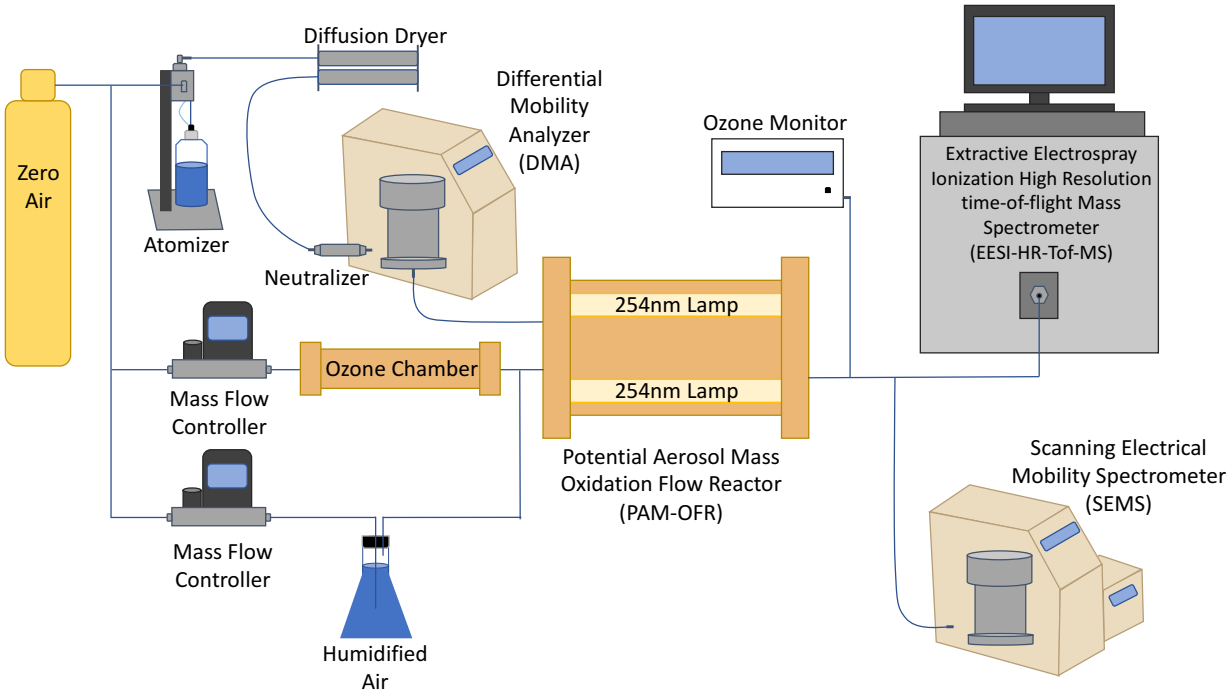

Figure 5. Schematic of the experimental setup using a PAM-OFR to simulate OH heterogeneous oxidation, an EESI-HR-ToF-MS to characterize product composition, and a SEMS to determine aerosol size distribution.

2.1 Atomizer

The TSI Model 3076 Constant Output Atomizer was used to aerosolize different triclosan solutions in the experiment. Figure 6 displays a schematic of how the atomizer operates. Compressed, filtered air is passed through an orifice and expands to create a high-velocity jet[74]. From the atomizer bottle attached below, the solution to be aerosolized is drawn up and becomes atomized by the high-velocity jet[74]. Large droplets impact the opposite wall and recirculate back to the atomizer bottle. The atomizer can be used in two different modes: (1) recirculation mode (for the least volatile solvents), whereby the solution that condensed on the wall drains back into

the atomizer supply bottle, and (2) non-recirculation mode (reserved for volatile solvents), whereby the condensed solution is drained into a separate waste bottle. The atomizer can generate up to ~10^7 particles cm^{-3} and the particle size generated can be adjusted by changing the concentration of the solution. The aerosolized sample exits from the outlet at the top and then becomes dried and neutralized prior to size selection.

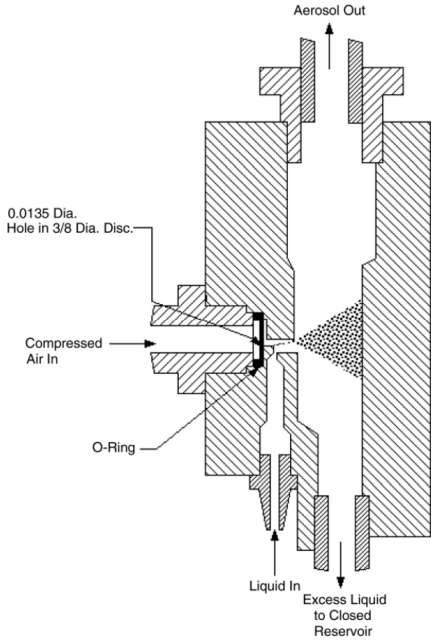

Figure 6. TSI Model 3076 Atomizer Schematic[75].

In the experiments, after the triclosan solution was aerosolized, the particles were dried by passing through the diffusion dryer. The dryer was equipped with an activated carbon denuder and silica beads. The activated carbon helps to remove volatile organic species from the flow stream while the silica beads dry the particles by absorbing water vapor.

2.2 Scanning Electrical Mobility Spectrometer

The scanning electrical mobility spectrometer (SEMS Model 2100, Brechtel) composed of a differential mobility analyzer (DMA), a mixing condensation particle counter (MCPC), and a system control box, measures aerosol size distribution and provides a source of monodisperse particles (see Fig. 7)[76].

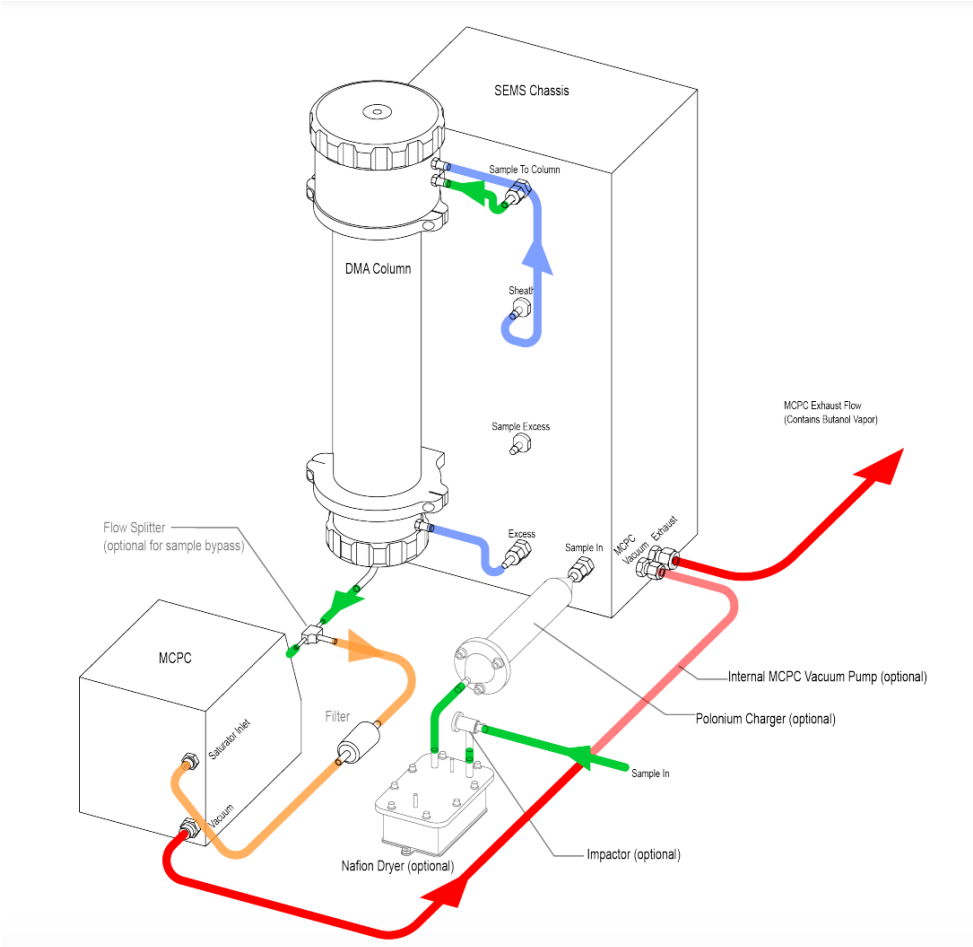

Figure 7. Schematic of the Brechtel Model 2100 SEMS[76].

Prior to aerosol size selection with the DMA, the sample flow passes through a neutralizer to reduce particle loss due to the electrostatic charges and to bring the particles to a steady-state charge distribution[74,75,77]. Upon interaction of gas molecules with the alpha particles that are emitted from the radioactive Polonium-210 strips in the neutralizer, bipolar-charged

gases are produced[76]. Aerosol particles that pass through the neutralizer then interact with the charged gasses and reach a known equilibrium charge distribution[76]. This is crucial for the DMA to effectively select charged particles as a function of their size[76]. Then, the DMA classifies aerosol particles according to their electrical mobility[78]. Figure 8 shows a schematic of the DMA. The sample aerosol flow encounters a sheath flow in the DMA and the electric field within the column is controlled by the charged center rod[78]. By altering the voltage applied to the center rod, and hence the electric field within the column, aerosol particles' electrical mobility diameter can be determined (see Eq. 4)[76]. Particle electrical mobility is calculated according to Eq. 4, where Z_p is the electric mobility (V/m^2s), n is the number of electrical charges carried by the particle, e is the units of electrical charge at 1.6×10^{-19}C, C_c is the Cunningham slip correction factor, μ is the air dynamic viscosity (kg/m s), and D_p is the particle diameter (m). The DMA center rod voltage is calculated according to Eq. 5, where V is the voltage applied to the DMA center rod (volts), Q_{sheath} is the sheath flow (m^3/s), R_{outer} is the outer cylinder inside radius (m), R_{inner} is the center rod outside radius (m), L_{DMA} is the center rod length (m), Z_p is the particle electrical mobility. At the selected voltage, high electric mobility particles will deposit on the center rod and low electric mobility particles will exit the column through the excess flow, only particles with a specific range of electric mobility will enter the selected sample flow and get counted by the MCPC[78]. The MCPC is a particle detector that counts the number of particles in each size bin sorted by the DMA[76]. An external vacuum pump draws a sample airflow of 0.36 LPM which becomes saturated with butanol vapor to reach droplet sizes that are detectable by the optical block[79]. The concentration of particles in each size bin is then calculated according to the level of light scattering detected[79].

$$Z_p = \frac{neC_c}{3\pi\mu D_p} \qquad \textit{Eq. 4}$$

$$V = \frac{Q_{sheath} \ln \frac{R_{outer}}{R_{inner}}}{2\pi L_{DMA} Z_p} \qquad \textit{Eq. 5}$$

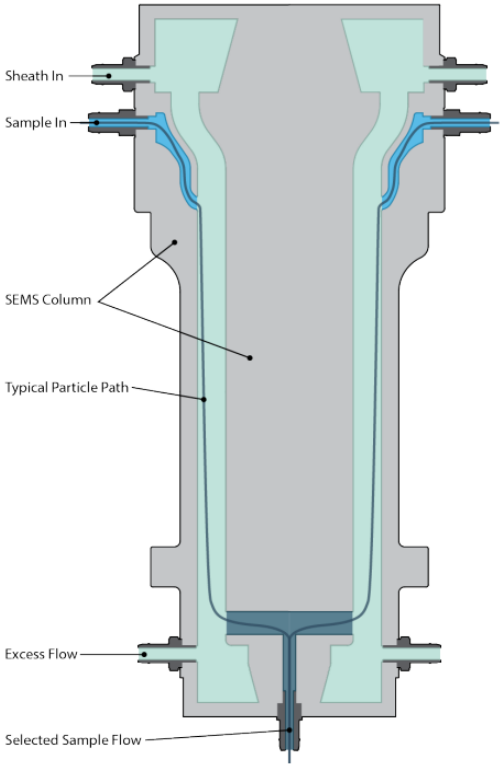

Figure 8. Schematic of DMA[76].

In this study, to generate monodisperse aerosol particles for degradation studies of triclosan, the sample flow was passed through a differential mobility analyzer (DMA). The DMA was set to size select at 200 nm. After chemical aging and photodegradation reactions were simulated in the PAM, the particle size distribution of the outflow was characterized using a SEMS. In a separate setup, the SEMS was used to calibrate the signal intensity of the EESI-HR-

ToF-MS for triclosan as a function of the aerosol mass concentration ($\mu g\ m^{-3}$) and to test the sensitivity as a function of triclosan particle size.

2.3 Potential Aerosol Mass Oxidation Flow Reactor

Potential aerosol mass oxidation flow reactors (PAM-OFR) are used in atmospheric chemistry studies to simulate chemical aging and atmospheric oxidation processes[80–82]. Unlike conventional environmental chambers, the PAM-OFR has a lower surface-area-to-volume ratio that reduces the effects of wall loss and provides shorter residence times from seconds to minutes[81]. The PAM-OFR generates high concentrations of oxidants at short residence times which allows for higher oxidant exposure and shorter experiment times[81].

The PAM-OFR, first introduced by Kang et al. 2007, is an aluminum cylinder with a volume of 13.3L and is 46cm long × 22cm wide. Two sets of low-pressure mercury lamps are enclosed in lamp sleeves placed in the reactor[81–83]. To generate OH for photo-oxidation studies of aerosol particles, two methods can be employed. In OFR 254 mode, the lamps only emit at 254nm, therefore, an external ozone chamber is needed to supply ozone as a precursor for OH production (see Reactions 1-2)[83].

$$O_3 + hv_{254} \rightarrow O_2 + O(^1D) \qquad \textit{Reaction 1}$$

$$O(^1D) + H_2O \rightarrow 2OH \qquad \textit{Reaction 2}$$

In OFR185 mode, the lamps emit at both 185nm and 254nm wavelengths, and OH is generated in the following reactions described by Reactions 3 - 6[83]. The photolysis of O_3 generates additional OH in the same fashion as in OFR 254 mode.

$$H_2O + hv_{185} \rightarrow H + OH \qquad \textit{Reaction 3}$$

$$H + O_2 \rightarrow HO_2 \qquad \textit{Reaction 4}$$

$$O_2 + hv_{185} \rightarrow 2O(^3P) \qquad \textit{Reaction 5}$$

$$O(^3P) + O_2 \rightarrow O_3 \qquad \textit{Reaction 6}$$

OH generation is influenced by the concentration of ozone, water, and photon flux at 254 nm present[83]. OH exposure, which is the product of the OH concentration and experiment residence time, at different UV lamp voltages can be determined with calibration experiments by measuring the decay of trace gases due to reaction with OH.

In this experiment, the PAM-OFR was operated in the OFR 254 nm mode with ozone supplied by the external ozone chamber. The total flow rate through the PAM was 6 LPM which was equivalent to a residence time of around 2.22 minutes. Of the total flow rate, triclosan sample flow accounted for 2 LPM, humidified air accounted for 3 LPM, and dry filtered air was set at 1 LPM flowing through the ozone chamber then into the PAM. Nitrogen gas was flowed through the lamp sleeves to prevent heat and gas buildup.

Each trial ran approximately 3 hours with all lamps off initially to establish the initial triclosan EESI-HR-ToF-MS intensity and once more at the end to correct for drift in signal intensity over the duration of the experiment. Prior to starting the photodegradation and OH exposure studies, the PAM-OFR UV lamps at 254 nm and the external ozone chamber lamps were blasted at 10 V to stabilize the irradiance and prevent photon flux fluctuations during the experiment. For the triclosan heterogeneous oxidation by OH study, the ozone lamp in the external ozone chamber was set consistently between 1.7-2 V for five different OH exposures at increasing levels, which was controlled by varying the PAM-OFR UV lamp voltage. For the direct photodegradation study of triclosan, the same setup was followed using the same UV lamp voltages except the external ozone chamber lamps were turned off. To determine the OH

exposure at each PAM-OFR lamp setting, a calibration experiment was conducted to calculate the decay of carbon monoxide (CO) at different OH concentrations. The OH exposure calibration curve is shown in Fig. 9. The OH exposure levels were calculated according to Eq.6 based on the assumption of a pseudo first-order reaction. The rate constant for CO + OH (k_{OH+CO}) used in the calculation was $1.5 \times 10^{-13} cm^3/molec\ s$ at 298K and the days of equivalent aging was determined assuming daytime OH concentration to be $1.5 \times 10^6 molec/cm^3$ [82,84–86].

$$OH_{exp} = -\frac{1}{(k_{OH+CO})} \times \ln\left(\frac{CO}{CO_0}\right) \qquad \textit{Eq. 6}$$

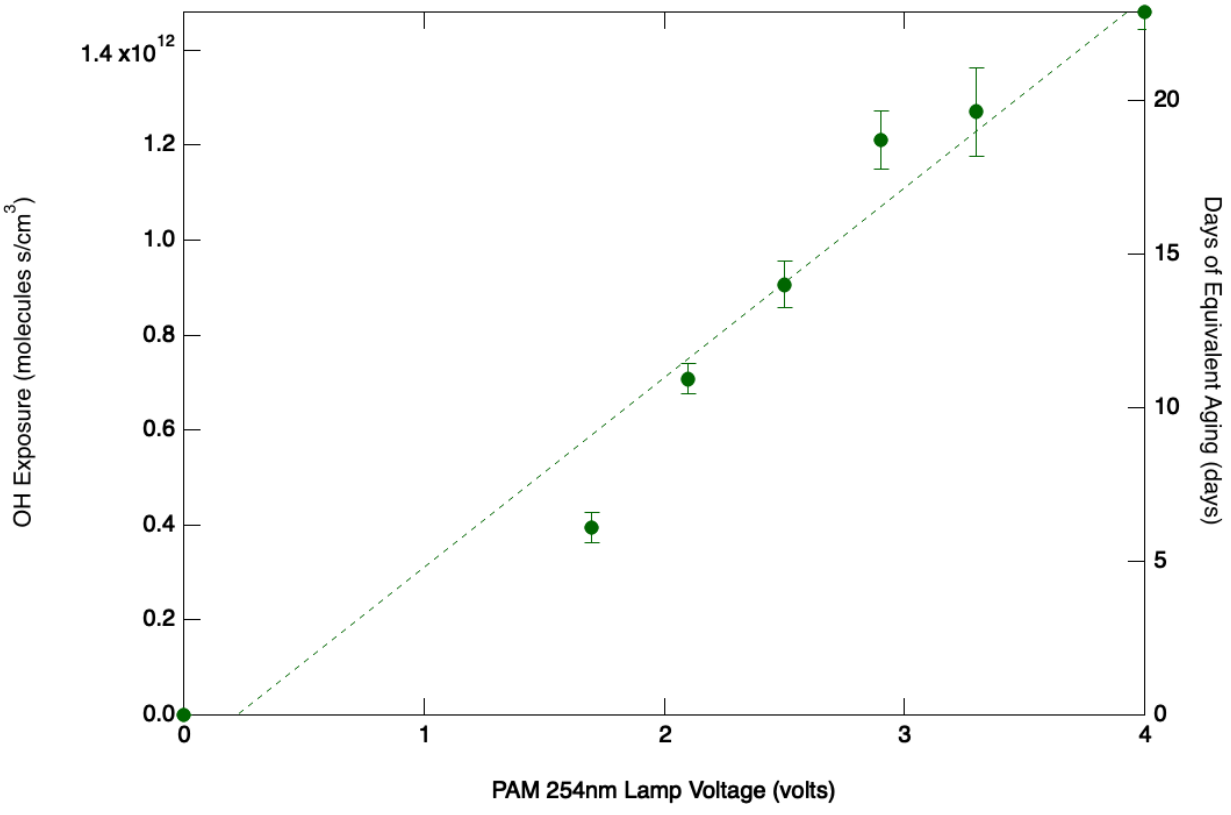

Figure 9. OH Exposure Calibration Curve.

A particular consideration for heterogeneous reactions that differ from analysis of homogeneous reactions is that "surface and condensed-phase reactions occur in the presence of solvent species."[105]. Interactions between solvent and gas-phase oxidants may result in scavenging effects that decrease the availability of OH to undergo oxidation reactions with triclosan[105]. In this study, due to the low solubility of triclosan in water, at a concentration of 10 mg/L[101], methanol was used as a cosolvent in making 200 ppm triclosan sample solutions. However, according to various studies on the influence of triclosan oxidation by OH, methanol can act as an OH scavenger[105]. To understand the potential effects of methanol on the concentration of OH in the PAM-OFR, the EESI-HR-ToF-MS signal for methanol (CH_3O^-, m/z = 31.0180) was monitored and compared among conditions with no OH present, lowest OH exposure level, and highest OH exposure level studied (see Fig. 10). No significant decrease in methanol signal was observed in the presence of OH. In addition, the signal for CH_3O^- may not be solely from the presence of methanol as it could also come from fragments of carboxylic acids during triclosan oxidation[68]. To limit significant water and methanol presence in the sample flow, aerosolized triclosan sample was dried by passing through a diffusion dryer equipped with activated charcoal and silica beads prior to entering the PAM-OFR. Additionally, the OH concentration was generated at high levels in the orders of $10^{11} - 10^{12}$molecules s/cm^3. Therefore, the presence of methanol as a solvent in this experiment was assumed not to exhibit significant OH scavenging effects.

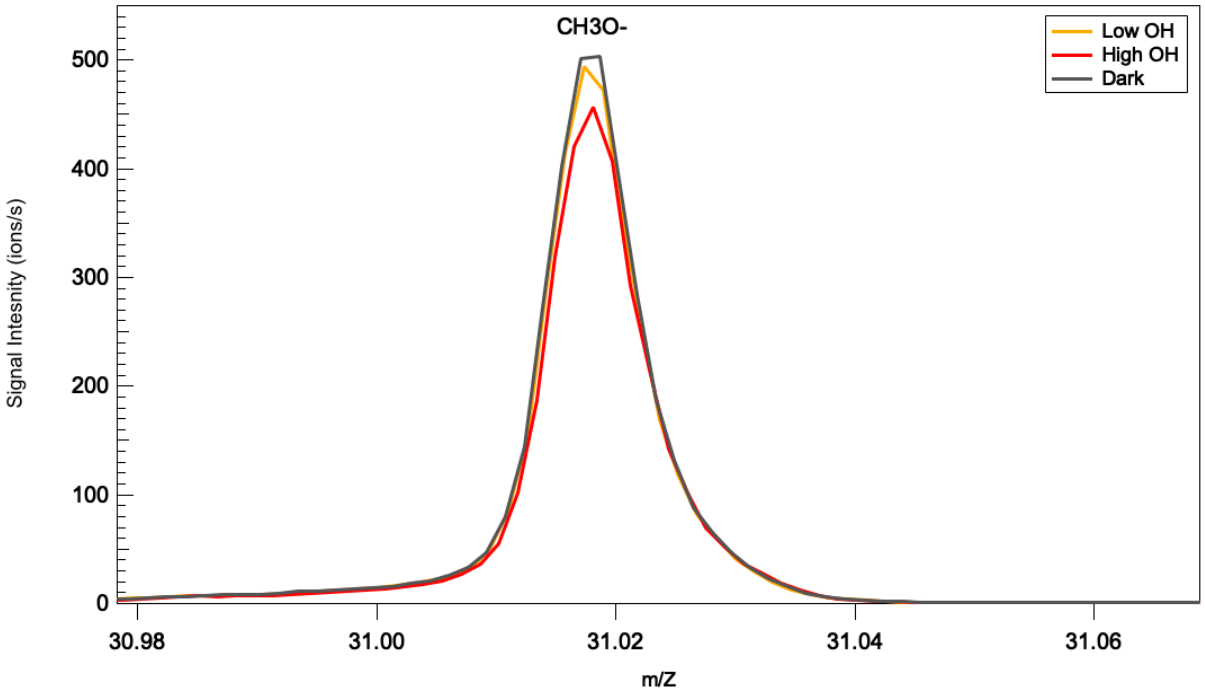

Figure 10. High resolution mass spectra for CH_3O^- in the presence of high OH exposure (depicted in red at an OH exposure of 1.21×10^{12}molecules s/cm^3), low OH exposure (depicted in yellow at an OH exposure of 1.03×10^{11}molecules s/cm^3), and no OH exposure (depicted in grey).

2.4 Ozone Monitor

An ozone monitor (Model 106-M, 2B Technologies) was used to measure the ozone concentration in the PAM-OFR at various levels of OH exposures. Since ozone is a precursor for OH formation, the concentration of ozone present in the PAM-OFR impacts the amount of OH generated. The ozone concentration was measured to monitor for consistency between different trials and to calibrate the OH exposure levels.

Figure 11 describes the schematic of the ozone monitor. Ozone concentration is measured based on how much UV light is absorbed with the amount of ozone molecules passing through the absorption cell[87]. An air pump, pulling at a flow rate of 1 LPM, draws the sample flow through the system[87]. The sample passes through a solenoid valve that alternates the flow between going through the ozone scrubber and bypassing it[87]. The purpose is to obtain

absorbance measurements for when there is no ozone present and when there is ozone present. Then, the sample enters the absorption cell, which is irradiated by a low-pressure mercury lamp at a wavelength of 254 nm as the light source. On the opposite end, a photodiode is used to detect the difference in absorbance for when there is ozone present and when there is no ozone present in the absorption cell[87]. The ozone concentration measured in molecules per cubic centimeter of sampled air is calculated using the Beer-Lambert Law (see Eq. 7)[87].

$$C_{O_3} = \frac{1}{\sigma l} \ln\left(\frac{I_0}{I}\right) \qquad \textit{Eq. 7}$$

C_{O_3} represents the ozone concentration (molecules/cm^3), σ refers to the ozone absorption cross section at 254 nm, l is the cell path length, I_0 is the ozone absorption intensity when the sample is scrubbed by the ozone scrubber, and I is the ozone absorption intensity when the sample bypasses the scrubber[87]. The pressure and temperature are also measured by the monitor to calculate the concentration of air molecules in the sample and, hence allows for the calculation of the ozone mixing ratio in parts per billion (ppb). Note that some interference by molecules that absorb at 254 nm is expected, e.g. H_2O_2, which could affect the measured $[O_3]$ and thus OH exposure. However, given $[O_3]$ is in excess, only a small percentage of the O_3 signal measured by the monitor is expected to result from such an interference.

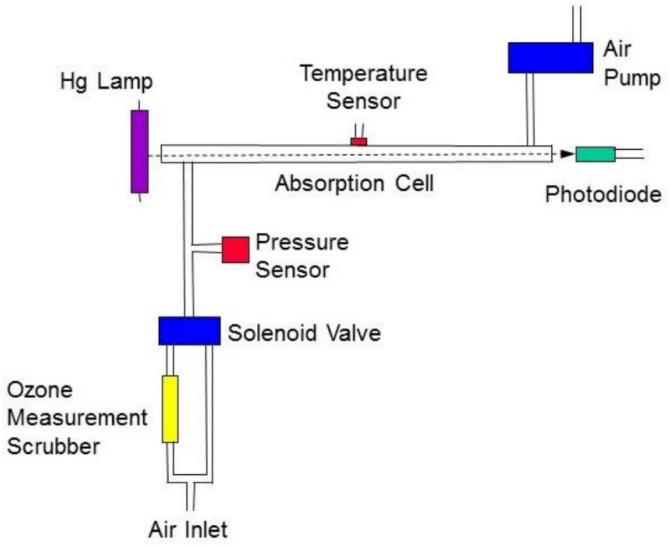

Figure 11. Schematic of the Ozone Monitor[87].

2.5 Extractive Electrospray Ionization High Resolution Time-of-Flight Mass Spectrometry

Extractive electrospray ionization high resolution time-of-flight mass spectrometry (EESI-HR-ToF-MS) is a field-deployable analytical technique that utilizes soft ionization to characterize chemical compounds in real-time[88]. Compared to offline aerosol measurement techniques, the EESI-HR-ToF-MS allows for significantly improved time resolution as no sample extraction is needed for aerosol characterization[88]. The soft ionization method of the EESI prevents particle fragmentation and decomposition that could complicate compound identification[88]. Thus, the molecular formula of organic aerosol measurements can be obtained[88].

The concept of EESI was first recorded by Cooks et al.[89]. Compared to ESI, EESI employs a dual-spray mechanism in which the nebulized neutral analyte becomes ionized after collision with a separate electrospray solvent[90]. With the EESI method, ambient, real-time sampling can be achieved by relying on liquid-liquid extraction of the two sprays[71]. The dual-spray mechanism evades problems that may arise from the presence of complex matrices, which

could lead to ion suppression[89,90]. Another advantage of using the EESI is that it allows for more options in ionization pathways, thus increasing its versatility by changing the solvent electrospray depending on the type of compound being analyzed[90]. Instrument sensitivity is significantly influenced by the mode of ionization and electrospray stability; therefore, spray optimization is crucial in maximizing instrument sensitivity[88]. With the EESI, positive ionization mode is commonly achieved with the addition of sodium iodide (NaI) in the electrospray to form sodium ion adducts[88,91]. Negative ionization mode has been studied using the addition of acetic acid or formic acid in the electrospray for the detection of deprotonated analytes[92,93].

With the EESI, the aerosol sample spray collides with the electrospray droplets that are charged with a high voltage and the droplets become ionized after evaporation of the soluble components[88,94]. Figure 12 shows a schematic of the EESI-HR-ToF-MS. Prior to collision with the electrospray solvent, the sample aerosol flow enters a denuder that removes gasses present, thereby reducing gas-phase background[88]. Then, the particle flow collides with a charged electrospray solvent that is delivered into a capillary by pressurized gas[88,95]. The electrospray-infused particle flow enters a heated manifold that evaporates the soluble components to form gas-phase ions through Coulomb explosion[88]. The ions then enter the HR-ToF-MS for analysis.

In the experiment, the EESI-HR-ToF-MS was used to measure triclosan degradation kinetics and identify the presence of triclosan transformation products. The EESI-HR-ToF-MS was used in negative mode to selectively monitor negatively charged ions. The electrospray solvent was composed of 100ppm NaI, 1% wt/wt glacial acetic acid, and 50:50 methanol to water. Under these conditions, triclosan was selectively ionized by acetate ions forming the deprotonated triclosan product, i.e., $[M-H]^-$ and acetic acid. NaI was added for mass calibration purposes, i.e., for high-resolution alignment of mass spectral peaks using I^-, I_2^-, and I_3^- as

representative mass calibrants. This increases the accuracy of peak identification during the characterization of triclosan and its transformation products.

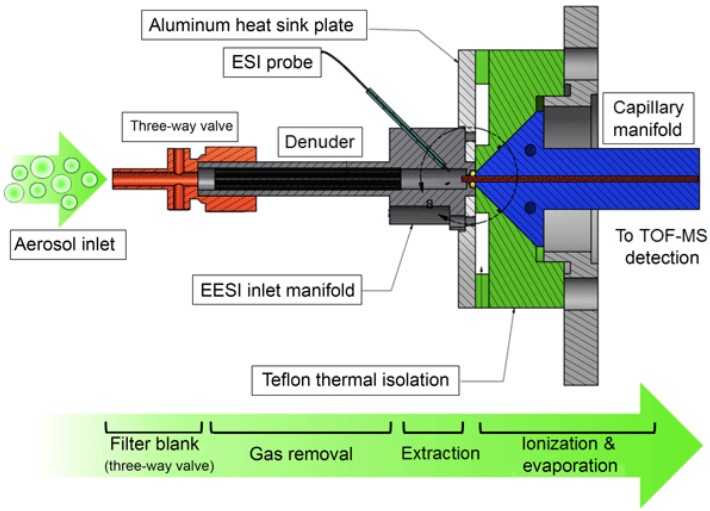

Figure 12. Schematic of the EESI-HR-ToF-MS. Image from Lopez-Hilfiker et al. 2019[88].

2.6 Uptake Coefficient Derivation

The kinetics of a heterogeneous or multiphase reaction can be described by the calculation of the reactive uptake coefficient, which is the ratio of the number of *reactive* gas-particle collisions to the total number of gas-particle collisions[64,96]. While the mass accommodation illustrates the processes of gas adsorption to particle surfaces and the uptake of adsorbed molecules into the bulk liquid, the reactive uptake demonstrates all the combined effects of the subsequent processes related to dissolution, bulk diffusion, and bulk reaction[64,96,97].

In this study, the reactive uptake of gaseous OH to triclosan particle surfaces is described by the effective uptake coefficient, which is represented as γ_{eff} in Eq. 8[98]. From heterogeneous oxidation experiments of triclosan, the uptake coefficient was calculated using the second-order rate constant (see Eq. 9)[65,99]. However, the diffusion of OH gas molecules through air can affect the rate of OH uptake at the aerosol surface. Therefore, to factor in the influence of OH gas phase diffusion on the uptake of OH by triclosan aerosol particles, a resistance formula with a

gas transport coefficient, Γ_{diff}, was incorporated into the uptake calculation to derive the effective uptake coefficient (see Eq. 10)[98]. The Knudsen number, K_n, which accounts for the transport of the gas molecules through air based on its mean free path, gas phase diffusion coefficient, and particle radius, was included in the correction (see Eq. 11)[98]. The diffusion-corrected reactive uptake coefficient equation is presented in Eq.12[98,100].

$$\frac{1}{\gamma_{\mathrm{eff}}} = \frac{1}{\gamma} - \frac{1}{\Gamma_{diff}} \qquad \textit{Eq. 8}$$

$$\gamma_{\mathrm{exp}} = \frac{2\mathrm{D}_0\rho_i\mathrm{N}_A}{3\bar{\mathrm{c}}_{OH}\mathrm{M}_i}(k_2) \qquad \textit{Eq. 9}$$

$$\frac{1}{\Gamma_{diff}} = \frac{(0.75 + 0.286\mathrm{K}_n)}{\mathrm{K}_n(\mathrm{K}_n + 1)} \qquad \textit{Eq. 10}$$

$$K_n = \frac{3\mathrm{D}_{OH}}{\bar{\mathrm{c}}_{OH}\mathrm{r}} \qquad \textit{Eq. 11}$$

$$\frac{1}{\gamma_{\mathrm{eff}}} = \frac{1}{\gamma_{\mathrm{exp}}} - \frac{(0.75 + 0.286\mathrm{K}_n)}{\mathrm{K}_n(\mathrm{K}_n + 1)} \qquad \textit{Eq. 12}$$

$\mathrm{D}_0 = \text{Surface area} - \text{weighted diameter}$
$\rho_\mathrm{i} = \text{Density of organic compound}$
$\mathrm{N}_\mathrm{A} = \text{Avogadro's number}$
$\bar{\mathrm{c}}_{\mathrm{OH}} = \text{Mean molecular speed of OH}$
$\mathrm{M}_\mathrm{i} = \text{Molecular weight of the organic compound}$
$\mathrm{S}_\mathrm{a} = \text{Surface area density}$
$\mathrm{r} = \text{Particle radius}$

Chapter 2, in part, coauthored with Slade, Jonathan H., is currently being prepared for submission under the title, "Photodegradation and heterogeneous OH oxidation kinetics and products of triclosan in sea spray aerosol mimics." The thesis author is the primary author of this chapter.

Chapter Three: Results and Discussion

3.1. Detection and Analysis of Triclosan and Photoproducts with EESI-HR-ToF-MS

3.1.1 Mass Spectra for Triclosan Isotopes

Triclosan in the aerosol phase was detected by negative ionization mode EESI-ToF at its specific mass-to-charge ratio (m/z) associated with the formula, $C_{12}Cl_3H_6O_2^-$, and confirmed via its isotopic pattern (see Fig. 13). In an aqueous phase triclosan photodegradation study conducted by Wong-Wah-Chung et al. 2007, they experimented with both positive and negative modes using electrospray ionization and found detection of triclosan and its products to be more sensitive in the negative mode[101]. They attributed the higher sensitivity to the hydroxyl group present in triclosan that allows the molecule to be more easily deprotonated[101]. Kliegman et al. 2013, who studied the involvement of radicals in triclosan phototransformation, were also able to detect triclosan and four of its primary photoproducts in negative mode electrospray ionization[102]. Therefore, in this study, the negative mode was selected for the characterization of triclosan and its photoproducts.

The aerosol-phase concentration of triclosan during the experiments was monitored based on the total (integrated) signal intensities of its associated isotopes. The contribution of chlorine and carbon isotopes in triclosan characterization can be observed in the mass spectra shown in Fig. 13. Peak intensities that arise from the presence of chlorine isotopes are especially apparent due to their natural abundance of 75.77% for ^{35}Cl (e.g., m/z~287) and 24.23% for ^{37}Cl (e.g., m/z~289) [101]. Additionally, this isotopic signature becomes important in the identification of chlorine-containing photoproducts.

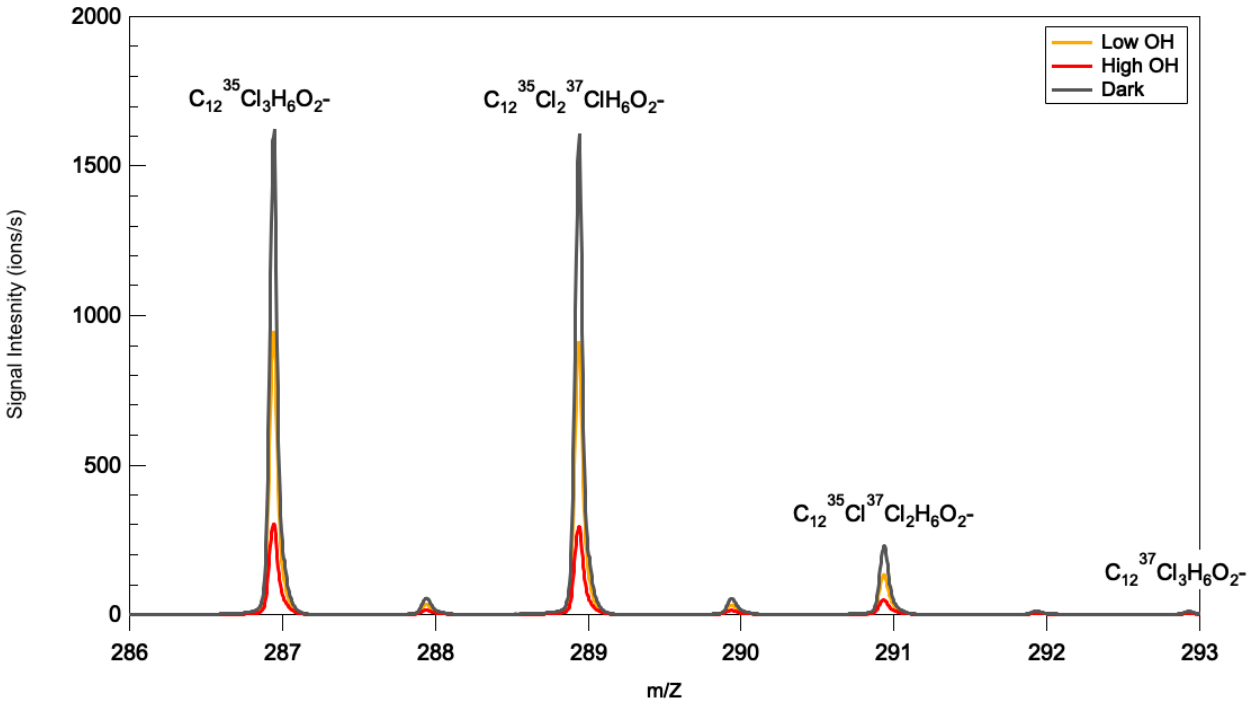

Figure 13. High resolution mass spectra for triclosan ($C_{12}Cl_3H_6O_2^-$) in the presence of high OH exposure (depicted in red at an OH exposure of 1.21 $\times 10^{12}$molecules s/cm^3), low OH exposure (depicted in yellow at an OH exposure of 1.03 $\times 10^{11}$molecules s/cm^3), and no OH exposure (depicted in grey).

3.1.2 Triclosan EESI-HR-ToF-MS Calibration Curve

To further assess the viability of employing the EESI-HR-ToF-MS to quantify triclosan degradation in the aerosol phase, the linearity between triclosan aerosol mass concentration and its signal intensity was graphed and analyzed in Fig. 14. Triclosan aerosol was generated with the atomizer and monodispersed at different diameters, including 100 nm, 150 nm, and 200 nm, using the DMA. As indicated in the calibration curve (see Fig. 14), triclosan signal responded linearly, across the three different diameters, with increasing mass concentrations measured from 0.2 to 14.6 μg m^{-3}. This conclusion is in line with the results obtained by Lopez-Hilfiker et al. 2019 and Gallimore and Kalberer et al. 2013 who observed an EESI linear response to organic aerosol mass concentration over the tested range of 0.01 to 1.00 μg m^{-3} and 3 to 600 μg m^{-3}, respectively[88,94]. Based upon the standard deviation of filter blanks, the aerosol mass

concentration limit of detection (3 ×standard deviation of blank) for triclosan was determined as ~0.006 μg m^{-3} and the limit of quantification ~0.02 μg m^{-3} for 100 nm-sized particles. The calibration curve result indicated that the EESI-HR-ToF-MS is effective at detecting small changes in aerosol mass concentration[94]. However, a decrease in EESI-HR-ToF-MS sensitivity was observed for triclosan with increasing particle size. In this experiment, the highest sensitivity was correlated to triclosan particles size-selected at 100 nm while the lowest sensitivity was correlated to triclosan size-selected at 200 nm (see Fig. 14). This result is contrary to those observed by Lopez-Hilfiker et al. 2019 and Gallimore and Kalberer et al. 2013 who found aerosol signal to be independent of particle size less than 200 nm for single-component organic aerosol particles[88,94]. The size-dependency of triclosan signal can be attributed to a decreased extraction efficiency with increasing particle size[88]. Lopez-Hilfiker et al. 2019 stated that larger aerosol particles, which approach the size of the electrospray droplets, may demonstrate less efficient extraction due to incomplete dissolution in the electrospray[88]. This phenomenon is further supported by the findings of Lee et al. 2021, who confirmed that EESI-HR-ToF-MS sensitivity is driven by the coagulation efficiency between the particle and the electrospray solvent[103]. From the results of Lee et al. 2021, an increase in EESI-HR-ToF-MS sensitivity as particle size decreased was also observed for nebulized levoglucosan, ammonium nitrate, and sucrose[103].

A note to mention for this study is that the DMA was set to size-select at 200 nm. This setting was chosen because, from size distribution analysis of monodispersed aerosol output from the DMA, the actual size distribution recorded by the SEMS downstream was shifted to smaller particles. During these experiments, size-selecting at 200 nm with the DMA generated particles with a surface area weighted diameter closer to around 134 nm, while size-selecting at

100 nm generated particles with a diameter closer to around 54 nm (see Fig. 15). The "shrinking" size of triclosan aerosol particles as they transport in the sampling lines could be due to partitioning of semi-volatile triclosan from the particle phase to the gas phase as is known for other semi-volatile aerosols[104]. Since aerosol particles in the accumulation mode, between the size range of 0.1 to 1µm, are associated with a prolonged lifetime in the atmosphere, they are more susceptible to heterogeneous reactions[105].

In summary, from the EESI-HR-ToF-MS calibration curve (see Fig. 14), it can be concluded that triclosan signal intensity correlates linearly with its mass concentration while the sensitivity exhibits a strong triclosan particle size dependence.

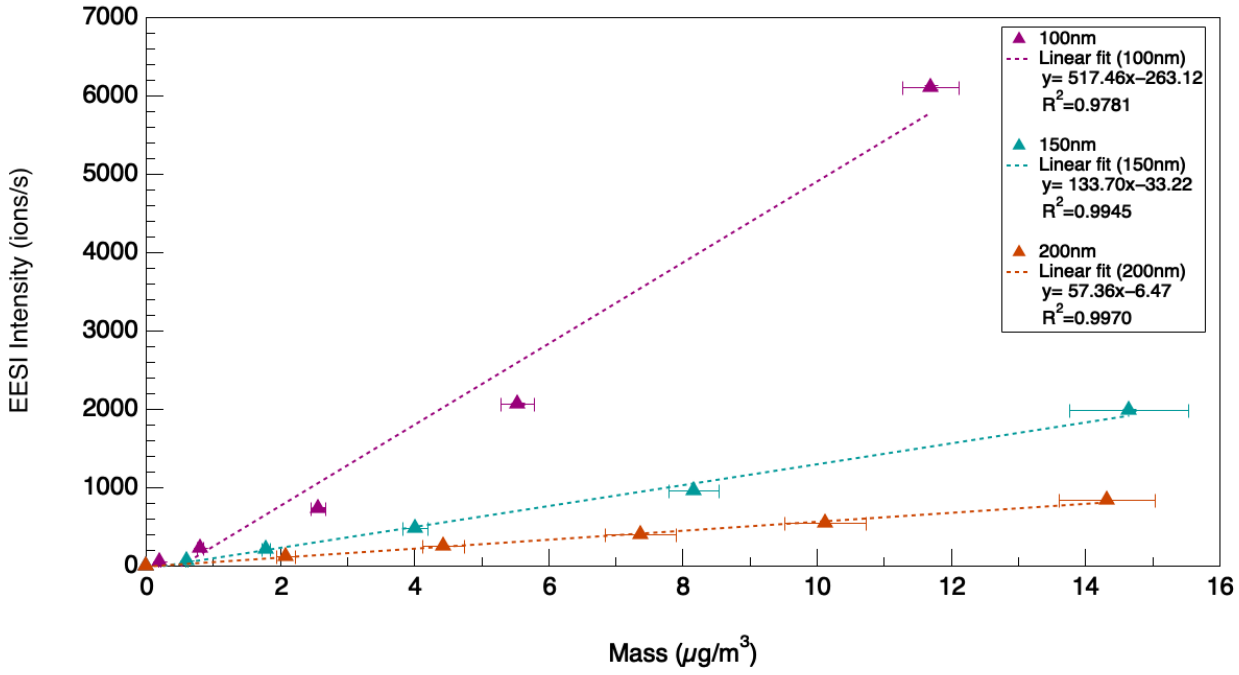

Figure 14. Calibration curve for aerosolized triclosan monodispersed in the size ranges of 100nm (purple), 150nm (green), and 200nm (orange), indicating the linear correlation between triclosan aerosol mass concentration and EESI-HR-ToF-MS triclosan signal.

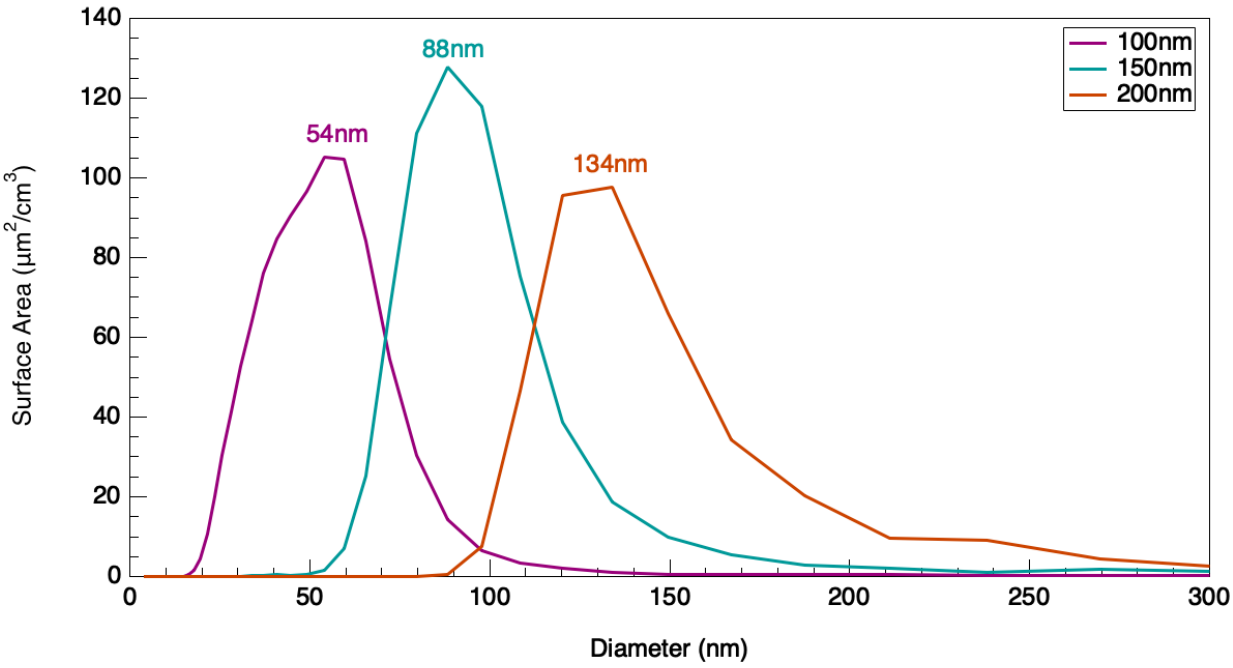

Figure 15. Size distribution of DMA monodispersed triclosan aerosol at 100nm (purple), 150nm (green), and 200nm (orange) measured by the SEMS.

3.1.3 Triclosan Degradation and Photoproduct Formation Time Series

For qualitative analysis of triclosan degradation using the EESI-HR-ToF-MS, a time series following an OH oxidation experiment of triclosan in the aerosol phase is shown in Fig. 16. Five different OH exposures with increasing levels were explored. Initial triclosan signal, without the influence of light or OH, in the PAM-OFR was established in the beginning. Humidified air and external ozone also flowed separately into the PAM-OFR for OH generation. Subsequently, the PAM-OFR 254nm lamps and external ozone lamps were turned on to 10 v to stabilize the lamp output. The UV irradiance and ozone blast at 10 v is marked in Fig. 16 by a significant decrease in triclosan signal intensity. Then, the 254 nm lamp voltage was increased incrementally from 1.7 v to 2.9 v to achieve five different increasing OH exposure levels ranging from 1.03×10^{11} molecules s/cm^3 to 1.21×10^{12} molecules s/cm^3. Increasing OH exposure

correlated to decreasing triclosan signal measured by the EESI-HR-ToF-MS as indicated in Fig.16. Lastly, the initial condition in the PAM-OFR was reestablished to determine how much of the change in initial triclosan signal was due to photodegradation and oxidation reactions as opposed to other external factors such as signal drift. The slight downward drift between the initial triclosan signal in the dark PAM-OFR and the final triclosan signal in the dark could be due to changes in solution concentration in the atomizer or wall loss interferences occurring inside of the PAM-OFR. The drift was linearly corrected over the course of the experiment for kinetics calculation to exclude the effects of potential external factors on triclosan signal. The time series showing the decrease in triclosan intensity with increasing OH exposure reveals the effectiveness of the EESI-HR-ToF-MS for monitoring real-time changes in triclosan signal due to heterogeneous oxidation by OH in the aerosol phase for the time scales of this experiment.

From the same triclosan oxidation experiment, a photoproduct was identified at the unit mass of m/z = 251 with a corresponding formula of $C_{12}Cl_2H_5O_2^-$ in negative ionization mode. The isotopic pattern of the presence of two chlorine substituents and the increase in molecule signal intensity with increasing OH exposure aided in the identification of the photoproduct. Previous studies have identified 2,8 dichlorodibenzo-*p*-dioxin (2,8 DCDD) to be a major photolysis product of triclosan in the aqueous phase[24,68,72,102]. Other products with the same formula, such as 2,7 DCDD and dichlorohydroxydibenzofuran were also identified in other triclosan photodegradation studies[67,106]. Therefore, the identity of the product could not be confirmed as the high-resolution EESI mass spectrometer does not elucidate structural information of the molecule. Offline analysis using liquid chromatography tandem mass spectrometry could be used to separate isotopes and confirm the structures of these photoproducts. From Fig. 17, clear generation of the photoproduct is observed with increasing

OH exposure. During the UV and ozone lamp voltage blast, there was a significant increase in the signal intensity of the photoproduct, $C_{12}Cl_2H_5O_2^-$. Increasing OH exposure levels and triclosan degradation corresponded to photoproduct formation. When the 254 nm and external ozone lamps were turned off, the signal intensity of the photoproduct decreased to background levels. The time series detailing the correspondence between triclosan degradation and photoproduct formation confirms the feasibility of using the EESI-HR-ToF-MS as an analytical tool to monitor real-time aerosol composition of triclosan and its transformation products. Proposed mechanistic pathways for photoproduct formation are highlighted in later sections.

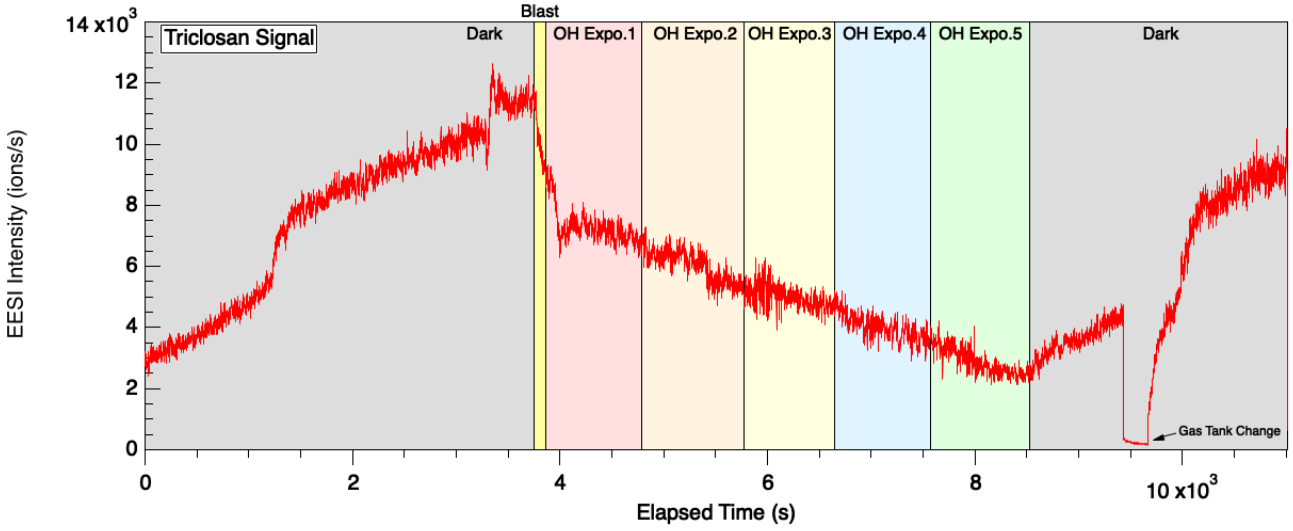

Figure 16. EESI-ToF-MS time series for triclosan ($C_{12}Cl_3H_6O_2^-$) during dark and five levels of OH exposure conditions. Blast indicates the condition in which the PAM OFR lamps and the ozone lamp were set to 10v to achieve stable irradiance. OH Expo.1 indicates an OH exposure level of 1.03×10^{11} molecules s/cm^3. OH Expo.2 indicates an OH exposure level of 3.95×10^{11}molecules s/cm^3. OH Expo.3 indicates an OH exposure level of 7.08×10^{11}molecules s/cm^3. OH Expo.4 indicates an OH exposure level of 9.06×10^{11}molecules s/cm^3. OH Expo.5 indicates an OH exposure level of 1.21×10^{12}molecules s/cm^3.

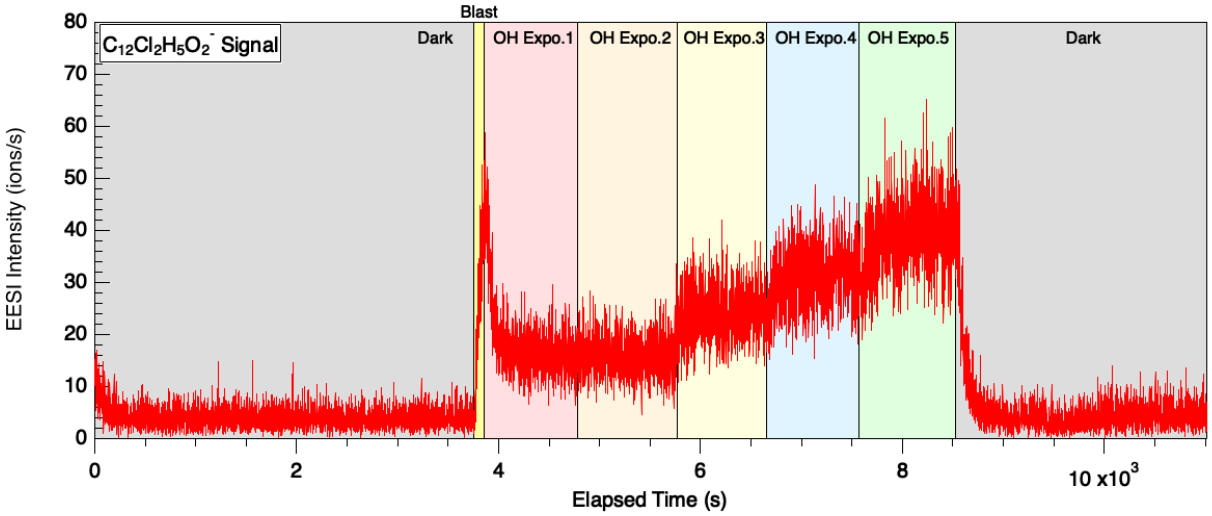

Figure 17. EESI-ToF-MS time series for $C_{12}Cl_2H_5O_2^-$, during dark and five levels of OH exposure conditions. Blast indicates the condition in which the PAM OFR lamps and the ozone lamp were set to 10v to achieve stable irradiance. OH Expo.1 indicates an OH exposure level of 1.03×10^{11} molecules s/cm^3. OH Expo.2 indicates an OH exposure level of 3.95×10^{11}molecules s/cm^3. OH Expo.3 indicates an OH exposure level of 7.08×10^{11}molecules s/cm^3. OH Expo.4 indicates an OH exposure level of 9.06×10^{11}molecules s/cm^3. OH Expo.5 indicates an OH exposure level of 1.21×10^{12}molecules s/cm^3.

3.2 Triclosan Degradation and Photoproduct Formation Kinetics

3.2.1 The Effects of UV Irradiance and OH Exposure

To understand the photodegradation and heterogeneous oxidation kinetics of triclosan in the aerosol phase, the effects of varying UV light irradiance and OH exposures on triclosan degradation are compared in Fig. 18. Change in the natural logarithm of triclosan signal intensities was plotted as a function of UV lamp irradiance, where I_t represents the average triclosan intensity measured by the EESI-HR-ToF-MS after photochemical reactions and I_0 represents the initial triclosan intensity with no light or OH present. The error bars represent the standard deviation between trials ranging from 6 - 11 trials conducted at each irradiance level. To isolate the effects of light on triclosan degradation, aerosolized triclosan was flowed into the PAM-OFR with a humidified air dilution flow and photolyzed under UV lamps

irradiating at a wavelength of 254 nm. With increasing levels of UV irradiance controlled by increasing the PAM-OFR lamp voltage, triclosan degradation increased. This result reveals aerosolized triclosan to be photolabile and readily degrades under the influence of UV irradiation in the PAM-OFR.

Various studies have found photolysis to be a major degradation pathway for triclosan in surface water[49,68,107]. The strong UV degradation characteristic of triclosan can be explained by its molecular structure and functional groups [39,108]. Triclosan is a chlorinated phenoxyphenol composed of a benzene ring, a phenolic ring, and three aryl chlorines[107]. Da luz et al. 2022 attributed triclosan's susceptibility to direct absorption of UV radiation to the presence of the phenol group, aryl chlorides, and weak C-H bonds in its chemical structure[108]. These functional groups may facilitate photochemical reactions through bond breakage[108]. Triclosan's susceptibility to photodegradation is also dependent on whether the molecule is present in its deprotonated, anionic form or its molecular form[108]. According to various triclosan degradation studies, experimental results indicated that triclosan in its deprotonated form, which is when the pH of the triclosan solution is greater than the pKa of triclosan (pKa around 7.9-8.2), is more efficient at light absorption than triclosan in its molecular form[24,39,101,109]. Mezcua et al. 2004 and Apell et al. 2020 observed the absorption spectra of triclosan in basic solutions to be red-shifted and, hence, contribute to greater overlap with the higher wavelengths of the solar spectrum[24,39]. In this study, the pH of aerosol particles was not directly measured. Triclosan solutions used for aerosolization, for single-component triclosan, binary-component triclosan + NaCl, binary-component triclosan + humic acid, and ternary-component triclosan + NaCl + humic acid, were measured to have a pH value less than the pKa of triclosan ~7.9-8.0 according to pH paper observations[39]. However, the pH of the aerosol particles that were irradiated could be different

than the solution pH as the aerosol sample stream was dried by passing through a diffusion dryer and a humidified dilution air stream was added. From these observations, it was preliminarily determined that the triclosan-containing aerosol particles undergoing photochemical degradation were acidic, therefore, existed in their molecular form in this study.

Additionally, Apell et al. 2020 discovered that the position in which the substituents are located on the chemical compound also influences the molecule's ability to undergo photolysis[39]. From studying lower chlorinated derivatives of triclosan, Apell et al. 2020 observed the chlorine attached para to the ether bond on the phenol side is critical for triclosan's environmentally relevant pKa, while the chlorine attached ortho to the ether bond on the benzene side is critical for dichlorodibenzo-*p*-dioxin and dihydroxylated biphenyl formation[39]. Chlorine on the phenol side withdraws electron density in the phenolate form and stabilizes the charge, contributing to the environmentally relevant pKa value of triclosan at 7.9-8.2[39]. Chlorine attached ortho to the ether bond on the benzene side is most favorable to undergo homolytic cleavage critical in DCDD formation pathways[39]. Therefore, the significant decrease in triclosan signal under the influence of 254nm irradiation observed in Fig. 18 could be attributed to the position of its functional groups and its presence in the phenolate or molecular form.

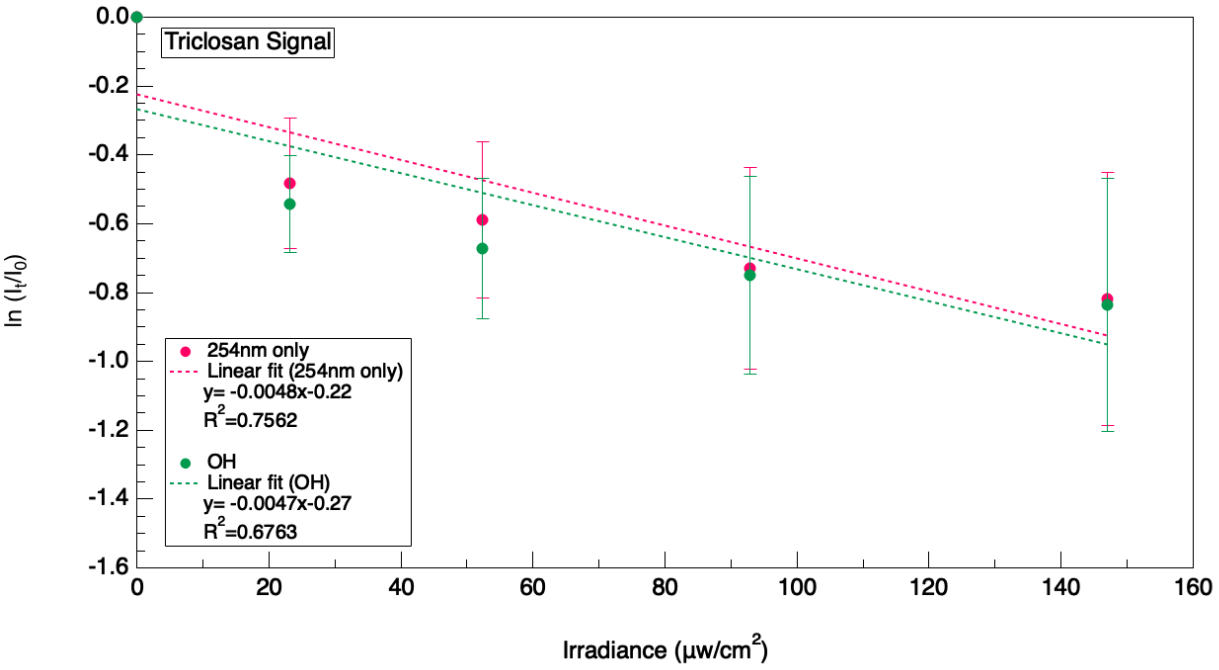

Figure 18. Degradation kinetics of triclosan in the presence of 254 nm UV light (red: 254 nm only) and the presence of OH radicals (green: OH+254 nm) as a function of PAM OFR lamp irradiance.

To compare the effects of OH heterogeneous oxidation on triclosan degradation, the change in triclosan signal due to increasing OH exposures is also represented in Fig. 18. The same experimental conditions to quantify the photolysis effects of triclosan were followed, except lamps in the external ozone chamber were turned on and ozone was added to the PAM-OFR for OH generation. Triclosan degradation results in this study indicated that exposure to OH does not lead to degradation rates that are statistically different from that because of UV irradiance alone.

In the presence of OH, triclosan can undergo OH addition or hydrogen abstraction, while electron transfer initiated reactions are found to be less spontaneous in comparison[107]. Gao et al. 2014 determined from quantum chemical calculations of OH-initiated reaction of triclosan in the aqueous phase that OH addition occurs most favorably at the carbon attached to the ether group

in the benzene ring while hydrogen abstraction occurs most favorably from the phenolic hydroxyl group[107]. OH-adducts and dehydrogenated radical generated will then undergo reactions to form more stable triclosan transformation products[107]. The type of transformation products formed could depend on the concentration of OH present, which influences reaction pathways[106,107]. As illustrated in Fig. 18, the non-linear decay of the log-normalized triclosan signal with increasing OH exposure could indicate mass transfer limitations between the particle surface and bulk that arise as the OH radical concentration increase[65,110]. It is also possible that heterogeneous OH oxidation had an insignificant impact on the concentration of triclosan in comparison to photodegradation due to the alteration of the triclosan aerosol surface by the buildup of less reactive photo/oxidation products. Oxidized reaction products exhibit rate constants that are significantly less (factor of two or more) than the starting reactant. In addition, the oxidized surface of organic aerosol particles can form viscous (crust-like) layers that slow molecular diffusion of gas-phase oxidants to the particle bulk while triclosan remains unreacted in the bulk. This would mean that as the OH exposure levels increase (i.e. as more of the aerosol oxidizes), uptake and reaction of OH by triclosan would decrease[65,111].

3.2.2 Triclosan Photoproduct Analysis

In this study, the photoproducts that exhibited a staircase trend of formation with increasing UV lamp voltage were identified at the unit mass of m/z = 251 and 253. Figure 19 shows the mass spectra of the peaks observed. These photoproducts were identified from high resolution mass spectrometry analysis and chlorine isotope patterns to have the molecular formula $C_{12}Cl_2H_5O_2^-$ and $C_{12}Cl_2H_7O_2^-$, respectively. Contribution to the signal intensity at m/z = 251 could be due to the presence of dichlorodibenzo-*p*-dioxin and/or hydroxylated

dichlorodibenzofuran (DCDD/F) (see Fig. 19)[67,102,106,107]. Contribution to the signal intensity at m/z = 253 could be due to the presence of dechlorinated triclosan (5-chloro-2-(4-chlorophenoxy)-phenol) and/or dihydroxylated dichlorobiphenyl ((OH)2PCB-13) (see Fig. 19)[39,101,102]. From free energy barrier calculations, Gao et al. 2014 determined that at low OH concentrations, DCDD can form from cyclization of dehydrogenated triclosan radical, but at high OH concentrations, OH-adduct formation dominates[107]. Furthermore, Zhang et al. 2015 determined from quantum chemical calculations in the gas phase that OH addition reactions lead to triclosan breakage to form mono-ring molecules[106]. The promotion of ether bond cleavage could hinder 2,8 DCDD formation that relies on photocyclization[38]. Kliegman et al. 2013 also noted that a biradical intermediate formation is important for the subsequent generation of the potential products, DCDD, dechlorinated triclosan, and dihydroxylated dichlorobiphenyl (see Fig. 20)[102]. Formation of the biradical from intramolecular electron transfer can be achieved under the influence of photolysis and is less spontaneous in OH-initiated reactions, further confirming the dominating effect of UV irradiance on triclosan degradation[102,107]. Therefore, analysis of the transformation products may elucidate the photochemical degradation pathways of triclosan in this experiment.

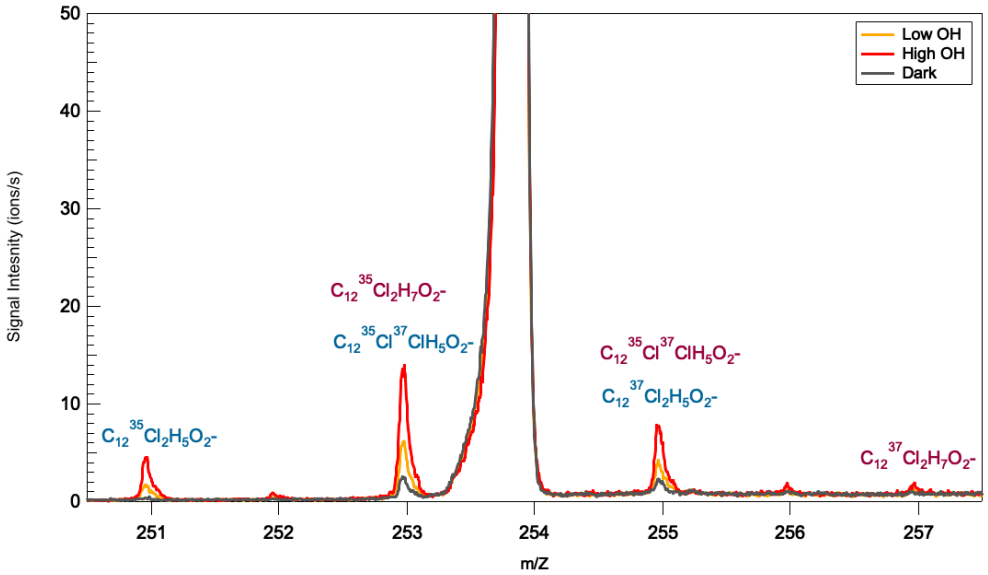

Figure 19. High resolution mass spectra for $C_{12}Cl_2H_5O_2^-$ and $C_{12}Cl_2H_7O_2^-$ in the presence of high OH exposure (depicted in red at an OH exposure of 1.21×10^{12}molecules s/cm^3), low OH exposure (depicted in yellow at an OH exposure of 1.03×10^{11}molecules s/cm^3), and no OH exposure (depicted in grey) (Signal intensity observed at 254 m/z is attributed to the presence of I_2^- present in the electrospray solvent for mass calibration purposes).

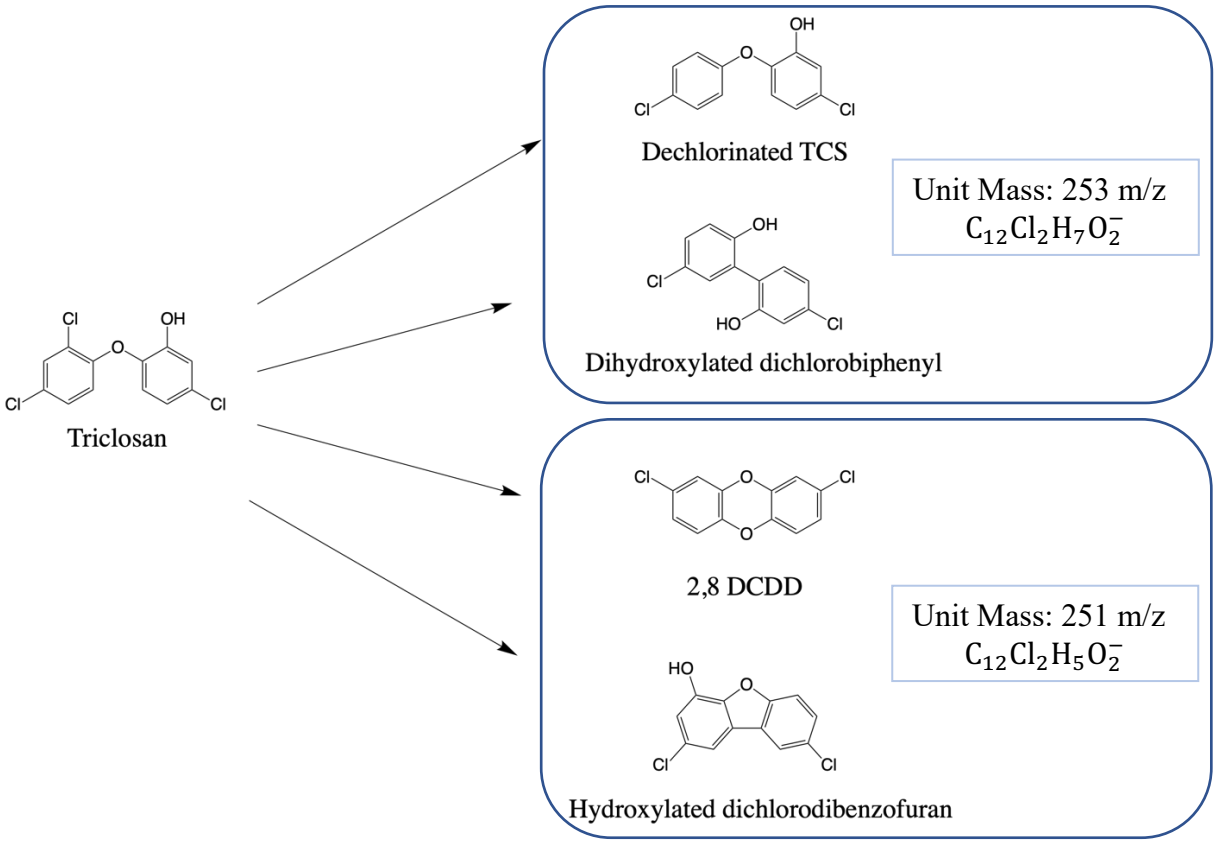

Figure 20. Potential triclosan photoproducts observed in mass spectra analysis (adapted from Kliegman et al. 2013)[102].

Formation kinetics of the photoproduct, $C_{12}Cl_2H_5O_2^-$, with a unit mass of m/z = 251 due to the influence of UV irradiance and OH exposure is compared in Fig. 21. According to the literature, 2,8 DCDD with the formula of $C_{12}Cl_2H_6O_2$ is a major transformation product widely observed in triclosan degradation in the aqueous phase[49,101,107]. Identification of DCDD is of particular interest due to its high toxicity[39,49,112]. Other products with the same molecular formula less frequently observed in studies are 2,7 DCDD and hydroxylated dichlorodibenzofuran[24,101,106]. However, hydroxylated dichlorodibenzofuran formation likely proceeds from H abstraction that occurs at the carbon ortho to the ether bond, which is less favorable compared to H abstraction from the phenolic hydroxyl group[106,107]. Therefore, it is postulated that the signal intensity observed at the unit mass of m/z = 251 is predominantly attributed to the formation of the DCDD photoproduct.

As shown in Fig. 21, DCDD formation increases with increasing UV irradiance and OH exposure. However, DCDD formation appears to be more favorable in the absence of OH, which indicates that the photocyclization pathway is more prevalent during photolysis than in OH oxidation reactions. Additionally, the formation of DCDD does not occur linearly. Formation of DCDD appears to plateau after initial generation at the lowest UV irradiance and OH exposure setting. This trend reveals the potential for DCDD to actively photodegrade under these experimental conditions. The characteristic of DCDD undergoing photolysis to generate secondary products was also observed in other studies [24,39,68]. In this study, the decrease in triclosan signal intensity is comparable between UV irradiance experiments and OH exposure experiments, however, the UV irradiance experiments appear to contribute to greater generation of DCDD/F due to the promotion of photocyclization pathways.

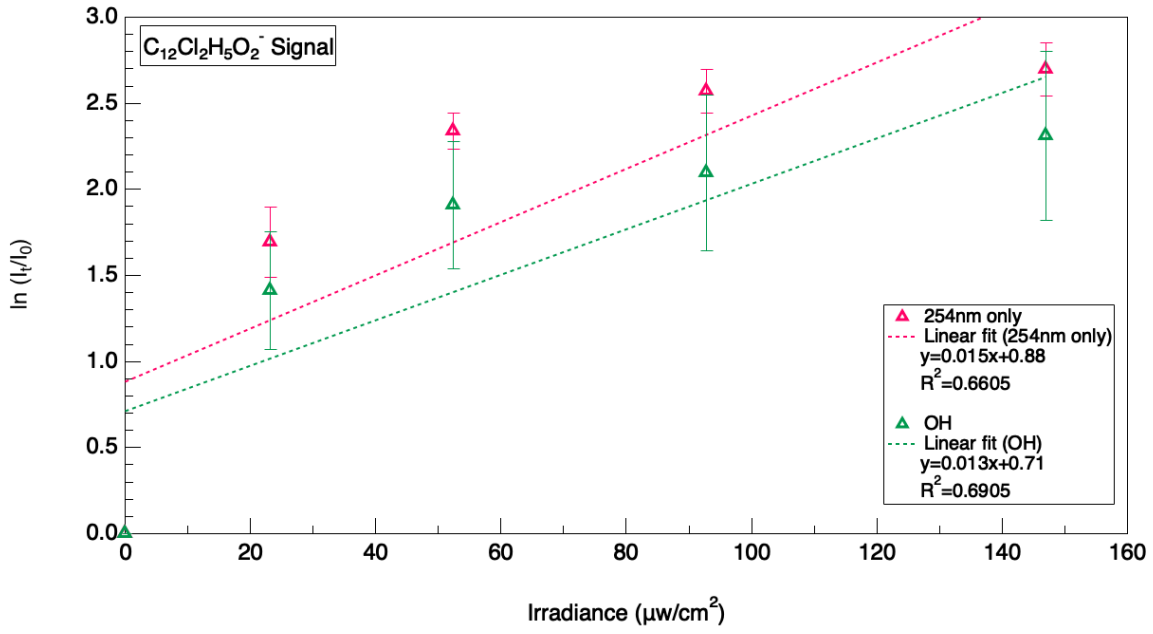

Figure 21. Photoproduct (DCDD), $C_{12}Cl_2H_5O_2^-$, formation kinetics in the presence of 254nm UV light (254nm only) and the presence of OH radicals (OH) as a function of PAM OFR lamp irradiance.

Degradation products identified in other studies due to triclosan ether bond cleavage include 2,4 dichlorophenol (2,4 DCP) and 4-chlorocatechol (4-CC)[38,106,107,112]. The presence of these potential photoproducts was also explored through mass spectrometry analysis in this study. Signal intensity of $C_6Cl_2H_3O^-$ at a unit mass of m/z = 161, potentially 2,4 DCP, is shown in Fig. 23. The signal at m/z = 161 appears to be the highest without UV irradiance or OH exposure, then decreases with increasing UV irradiance and OH exposure (see Fig. 23). This observation indicates that 2,4 DCP is present in the atomizer solution prior to aerosol formation, which is in line with records showing 2,4 DCP as a precursor in triclosan synthesis. The trend of decreasing signal intensity shown in Fig. 23 reveals that 2,4 DCP may undergo photodegradation due to the influence of UV irradiance and OH exposure. This observation is consistent with other studies that found 2,4 DCP to be photolabile[39,68,102]. Latch et al. 2005 calculated the degradation rate constant for 2,4 DCP to be two orders of magnitude greater than its formation rate constant,

which explains why the degradation of 2,4 DCP in these experiments is favored[68]. The photolysis of 2,4 DCP is suggested to form chlorocyclopentadiene carboxylic acid isomers, 3-chlorophenol, and 4-chlorocatechol (see Fig. 22)[38,39,49,68,113]. From mass spectra analysis for the potential product, chlorocyclopentadiene carboxylic acid with an assigned formula of $C_6ClH_3O_2^-$ at a unit mass of m/z = 143, the signal appears to decrease with increasing UV irradiance and OH exposure indicating further degradation (see Fig. 24). According to other studies, formation of 2,4 DCP from ether bond cleavage of triclosan can lead to the production of 3-chlorophenol (see Fig. 22)[49,102]. It has also been recorded to be a secondary product from 2,4-DCP photolysis[49,102]. In this study, the presence of 3-chlorophenol could not be confirmed. The unit mass of 3-chlorophenol at m/z = 127 coincides with the mass of iodide ion that was added in the electrospray for mass calibration. Another common product, 4-chlorocatechol (4-CC) with the formula $C_6ClH_4O_2^-$ at m/z = 143, observed from other triclosan degradation experiments is analyzed in the mass spectra shown in Fig. 25[108,112]. The presence of 4-CC cannot be confirmed from mass spectra analysis due to the low signal intensity observed at the corresponding unit mass. Various studies have also observed polymerization products from the photolysis of triclosan[38,39]. However, high molecular weight products due to the polymerization of triclosan under photolysis or heterogeneous oxidation were not observed in the EESI-HR-ToF mass spectra. From photoproduct analysis results obtained, EESI-HR-ToF-MS is shown to be a novel online analytical technique to qualitatively and quantitatively detect triclosan and its transformation products in the aerosol phase. From mass spectra analysis, it can also be concluded that the products, DCDD and 2,4 DCP, can serve as intermediates and undergo further degradation pathways to form smaller secondary products.

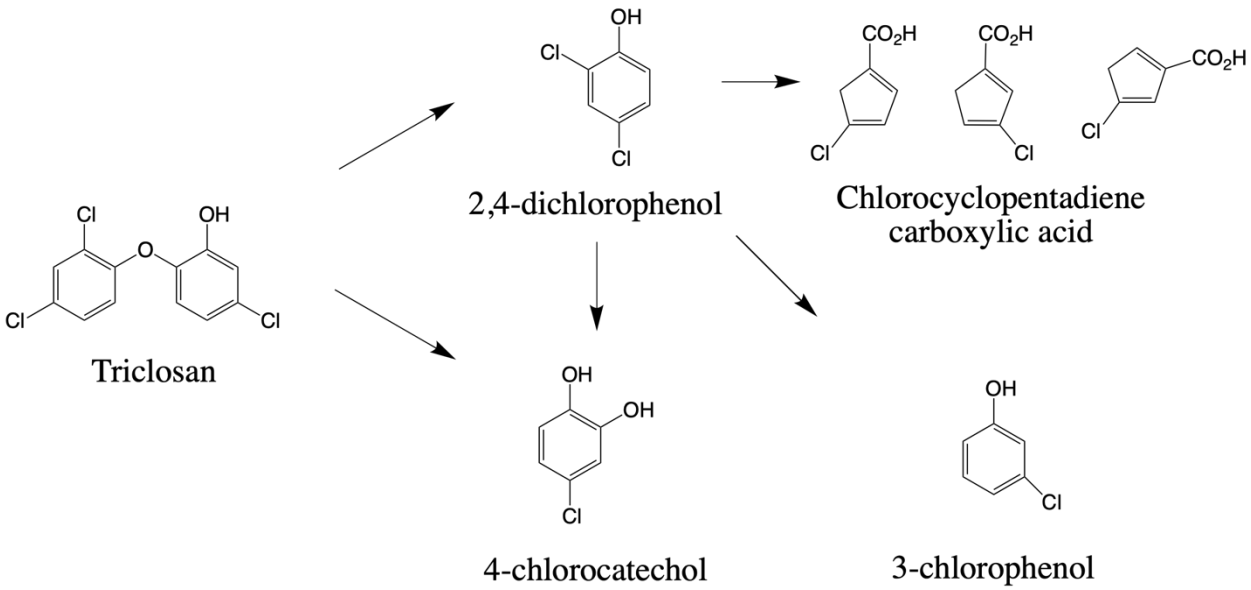

Figure 22. Potential triclosan photoproducts from ether bond cleavage pathway.

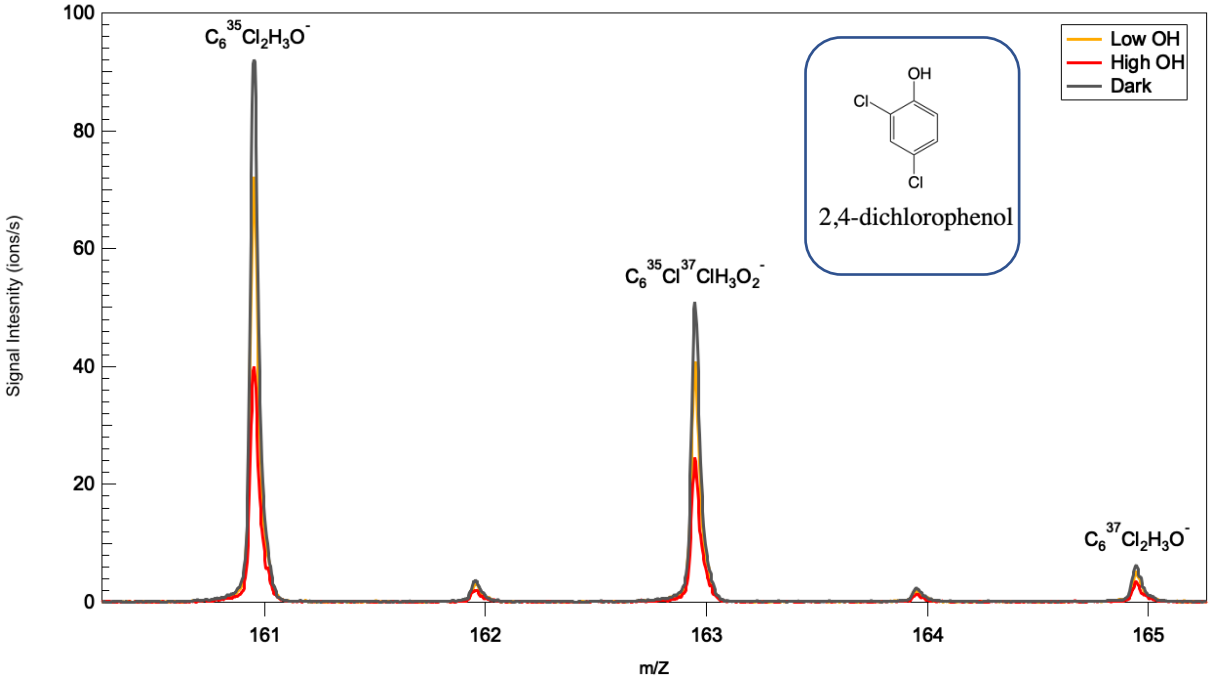

Figure 23. High resolution mass spectrum for $C_6Cl_2H_3O^-$ in the presence of high OH exposure (depicted in red at an OH exposure of 1.21 $\times 10^{12}$molecules s/cm^3), low OH exposure (depicted in yellow at an OH exposure of 1.03 $\times 10^{11}$molecules s/cm^3), and no OH exposure (depicted in grey).

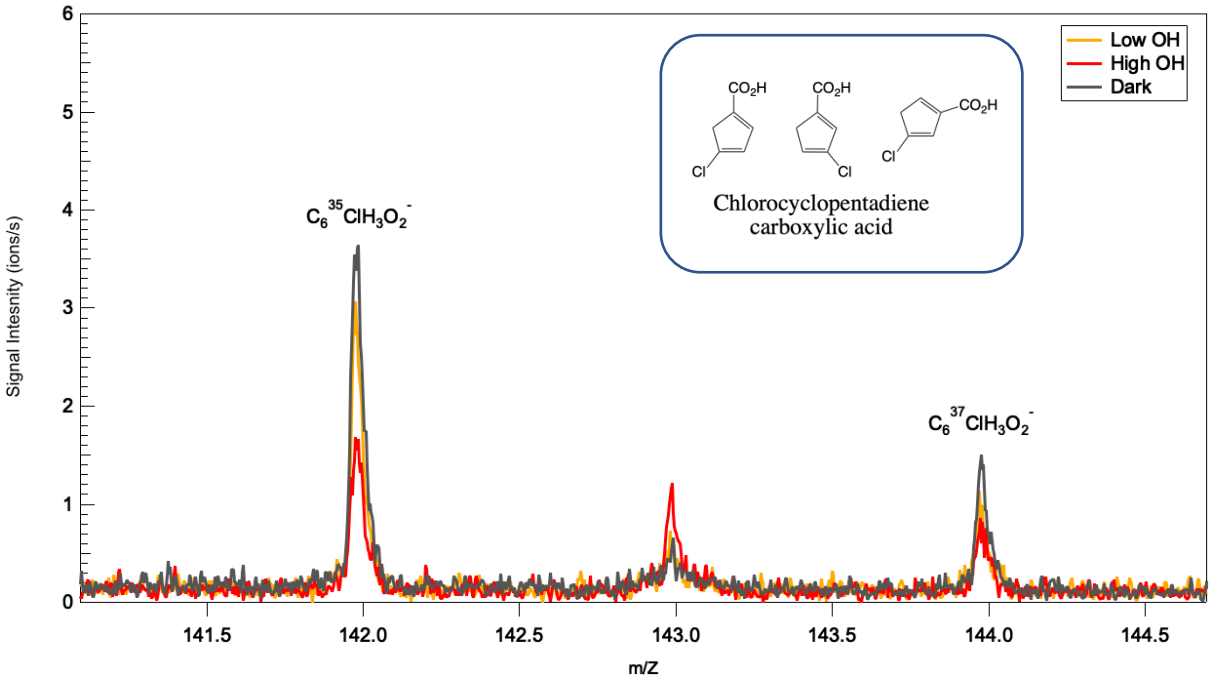

Figure 24. High resolution mass spectrum for $C_6ClH_3O_2^-$ in the presence of high OH exposure (depicted in red at an OH exposure of 1.21 $\times 10^{12}$molecules s/cm^3), low OH exposure (depicted in yellow at an OH exposure of 1.03 $\times 10^{11}$molecules s/cm^3), and no OH exposure (depicted in grey).

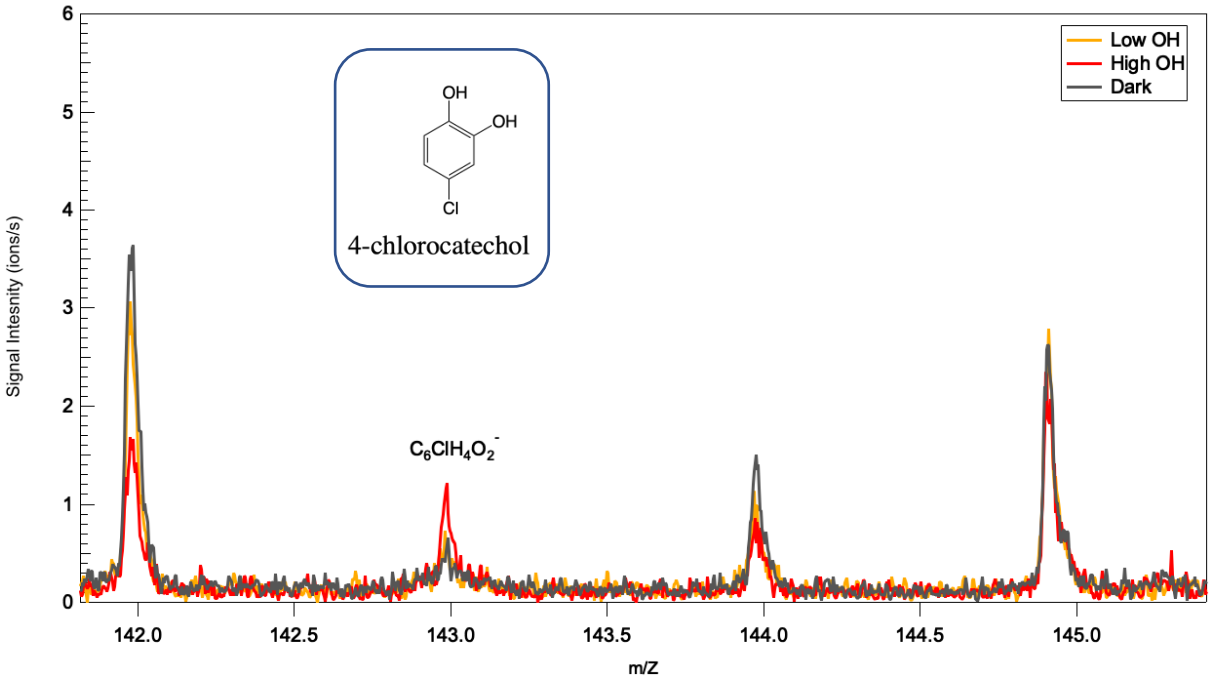

Figure 25. High resolution mass spectra for $C_6ClH_4O_2^-$ in the presence of high OH exposure (depicted in red at an OH exposure of 1.21 $\times 10^{12}$molecules s/cm^3), low OH exposure (depicted in yellow at an OH exposure of 1.03 $\times 10^{11}$molecules s/cm^3), and no OH exposure (depicted in grey).

3.2.3 The Effects of Humic Acid

The influence of humic acid, as a CDOM proxy, on triclosan heterogeneous oxidation in the aerosol phase was explored. Figure 26 shows the change in the natural logarithm of triclosan intensity as a function of OH exposure for systems with and without the addition of humic acid. Second-order rate constants were derived from the slope of the linear fit (see Table 1). From studying the OH heterogeneous oxidation of triclosan with and without humic acid, the second-order rate constants were determined to be $(5.74 \pm 1.40) \times 10^{-13}$ and $(2.97 \pm 1.25) \times 10^{-13}$ molecules s/cm^3, respectively. From averaged surface area-weighted diameters and second order rate constants, effective uptake coefficients were calculated to be 0.15 ± 0.04 and 0.09 ± 0.04 for systems without and with humic acid, respectively (see Table 1)[99]. The addition of humic acid decreased the effective uptake coefficient, alluding to decreased reactive collisions of OH in the gas phase and triclosan in the particle phase. Half-life of triclosan in the two systems was determined using Eq. 14 [114]. Daytime OH concentration was estimated at 1.5×10^6 molecules$/cm^3$ and half-life was calculated based on a 12-hour day assumption. In the presence of humic acid, the half-life of triclosan was increased to 36.05 ± 15.25 days from 18.63 ± 4.53 days in the absence of humic acid. As indicated in Fig. 26 and from the decreased uptake coefficient, heterogeneous oxidation of triclosan is hindered in the presence of humic acid in this study. This inhibition could be due to the OH scavenging and light absorption properties of humic acid[115,116].

$$t_{1/2} = \frac{0.693}{K_2[OH]} \qquad \textit{Eq. 13}$$

In the environment, CDOM can act as a photosensitizer and generate transient reactive species such as OH, singlet state oxygen, and CDOM in its triplet state from photochemical

reactions[49,109,117]. Studies conducted on the photodegradation of triclosan in the presence of humic acid in the aqueous phase observed enhanced triclosan degradation rates due to the photosensitizer properties of CDOM[37,109,118]. Chen et al. 2016 found the addition of humic acid to significantly enhance photolysis of triclosan in the molecular form, while degradation was inhibited for triclosan in the anionic form[49]. Similarly, Bianco et al. 2015 also found triclosan in the molecular form to actively react with OH and CDOM in the triplet state, but the effects of direct photolysis were more dominant for triclosan in the anionic form[109]. Results from literature indicate the presence of triclosan in the molecular form or the anionic form to be a significant factor in triclosan degradation kinetics in the presence of CDOM[49].

In this study, we did not observe an enhancement in the degradation of triclosan in the presence of humic acid, suggesting interactions between OH and humic acid interfered with triclosan heterogeneous oxidation with OH. CDOM has been described to be the main sink of OH in natural waters[109,119,120]. Huang et al. 2018 found CDOM to scavenge OH in triclosan oxidation processes due to a high second-order rate constant for reactions between CDOM and OH[121]. They explained that the OH scavenging effects were favored over OH production from CDOM photolysis[121]. Similar inhibition effects of CDOM were observed in this experiment. Another explanation for the inhibition effect is that the presence of CDOM can also screen UV light available for photolysis reactions of triclosan[115,116]. Chen et al. 2017 stated that the "total effect of the humic substance on organic contaminant degradation depends on the competing effects of light screening and photosensitization"[115]. As discussed in previous sections, triclosan is susceptible to undergo degradation from photolysis. Therefore, humic acid may have slowed degradation of triclosan because it absorbed the incoming light that would have otherwise photolyzed triclosan[109].

To further evaluate the attenuation effects of triclosan degradation due to the presence of humic acid, the rates of DCDD product formation were compared. As shown in Fig. 27, the presence of humic acid in the triclosan aerosol system inhibits the formation of DCDD. This result is in accordance with the findings of Chen et al. 2016 who observed that the addition of humic acid in triclosan aqueous systems decreased triclosan photodegradation rates and inhibited the formation of 2,8 DCDD[49]. The nonlinearity in triclosan degradation in the presence of humic acid was also observed. This result could be explained by the competing effects of photosensitization, light screening, and OH scavenger properties of CDOM[115]. At higher OH exposure levels, humic acid may participate in OH scavenging that hinders the degradation kinetics of triclosan[109]. Bianco et al. 2015 found the inhibition effect of CDOM to be higher for OH than for direct photolysis, which can explain why the formation rate of DCDD product decreased in the presence of humic acid and with increasing OH exposure[109].

Strong consensus on the effects of CDOM on triclosan degradation has not been established as the extent of triclosan degradation was shown to vary according to humic acid concentration and the pH of triclosan solutions[49,109,115]. In this study, the same suite of products was observed from mass spectra comparison for experiments conducted with and without humic acid. Therefore, it is postulated that triclosan degradation proceeds in similar pathways in the presence of humic acid.

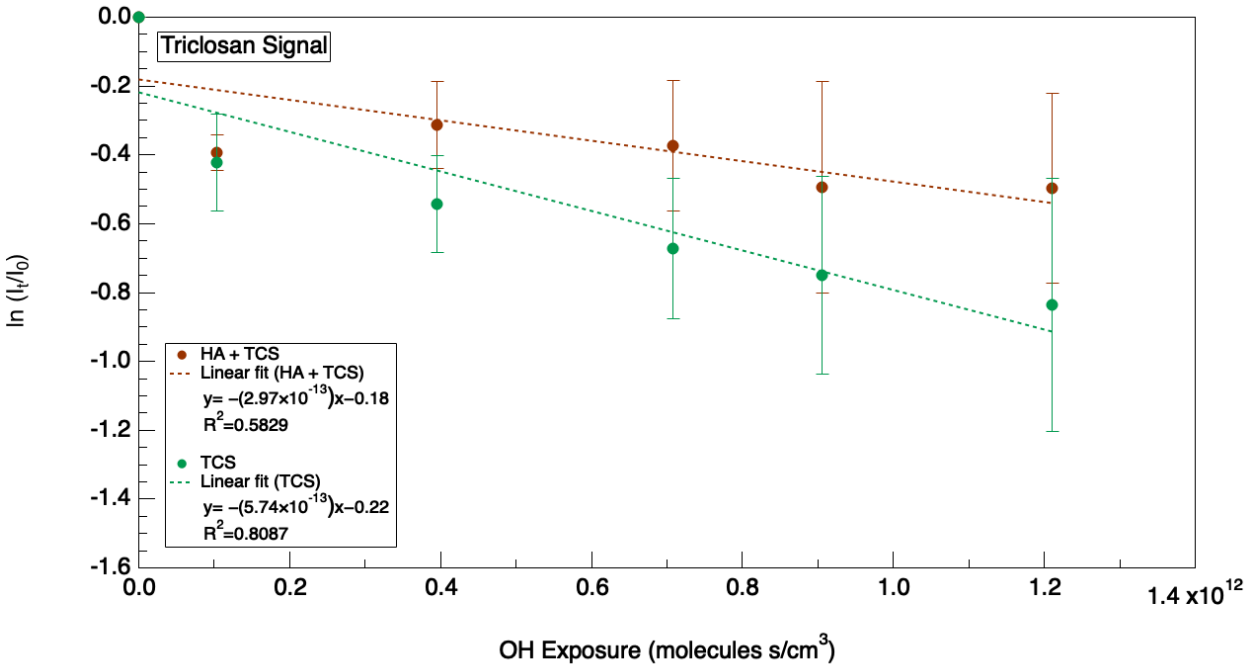

Figure 26. Triclosan degradation kinetics due to the addition of humic acid (HA) as a function of OH exposure.

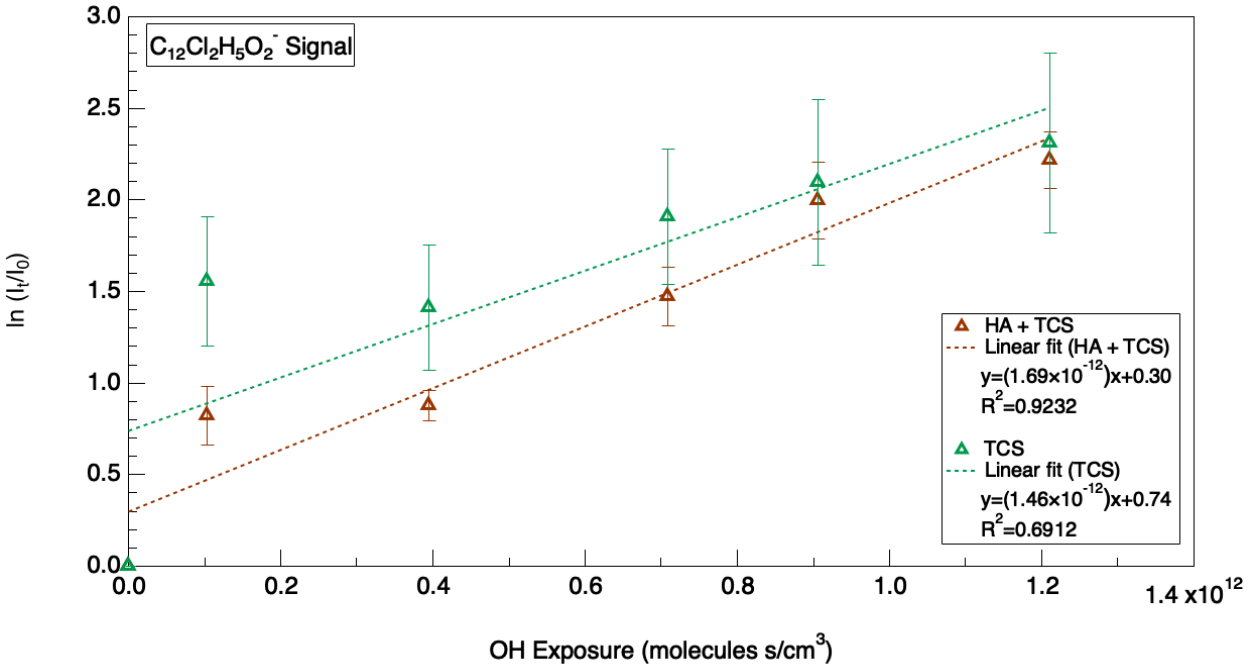

Figure 27. Photoproduct, $C_{12}Cl_2H_5O_2^-$, formation kinetics due to the addition of humic acid (HA) as a function of OH exposure.

Table 1. Effective OH reactive uptake coefficient, γ, for systems containing triclosan only (TCS), triclosan with NaCl (NaCl+TCS), and triclosan with NaCl and humic acid (NaCl+HA+TCS).

Aerosol System	$k_2 \left(\frac{cm^3}{molec \cdot s}\right)$	Particle Diameter (nm)	γ_{eff}	$t_{1/2}$(days)
Triclosan	$(5.74 \pm 1.40) \times 10^{-13}$	85.61 ± 8.10	0.15 ± 0.04	18.63 ± 4.53
Humic Acid + Triclosan	$(2.97 \pm 1.25) \times 10^{-13}$	903.57 ± 27.92	0.09 ± 0.04	36.05 ± 15.25
NaCl + Triclosan	$(5.41 \pm 1.39) \times 10^{-13}$	173.86 ± 39.08	0.29 ± 0.08	19.77 ± 5.10
NaCl + Humic Acid + Triclosan	$(5.48 \pm 1.09) \times 10^{-13}$	138.62 ± 28.08	0.24 ± 0.05	19.51 ± 3.90

3.2.4 The Effects of NaCl

In sea spray aerosol mimic studies, the influence of NaCl on the heterogeneous oxidation of triclosan was also explored. Figure 29 shows the change in the natural logarithm of triclosan intensity as a function of OH exposure for the binary-component triclosan + NaCl aerosol, ternary-component triclosan + NaCl + humic acid aerosol, and the single-component triclosan aerosol. Three trials were conducted as replicates for the NaCl-containing systems and the error bars represent the standard deviation between trials. The same methods for determining rate constants and half-lives as mentioned in the previous section were followed. The second-order rate constants were determined to be $(5.41 \pm 1.39) \times 10^{-13}$ and $(5.48 \pm 1.09) \times 10^{-13}$ molecules s/cm^3 for the system with NaCl and the system with both NaCl and humic acid, respectively. From our analysis of the second-order rate constants (i.e., the slope of the linear fits in Fig. 28) of the three aerosol systems reacting with OH, triclosan degradation and photoproduct formation kinetics were not significantly different between the three systems (see Fig. 28 and Fig. 29). However, when accounting for differences in heterogeneous reactivity due to differences in particle surface area between the three aerosol systems, mixtures containing

NaCl showed greater reactive loss of triclosan following uptake by OH. Uptake coefficients for the single-component triclosan aerosol, the binary-component triclosan + NaCl aerosol, and the ternary-component triclosan + NaCl + humic acid aerosol were $0.15 \pm 0.04, 0.29 \pm 0.08,$ and 0.24 ± 0.05, respectively.

The presence of NaCl in aerosols can lead to various contributions. In the aqueous phase, high concentrations of chloride (Cl^-) in seawater can lead to halogen radical formation that can further impact photochemical processes[122]. Potential pathways of radical formation include photolysis of free chorine and oxidation of chloride ions by OH and triplet state CDOM[122,123]. Due to chloride being a relatively large and polarizable anion, it can be more readily available at the particle surface, hence, increasing its surface reactivity with gaseous oxidants in the atmosphere[71,124]. The importance of interfacial reactions between chloride and gaseous OH was explored by Thomas et al. 2005 and Knipping et al. 2000, who found it to be a dominant pathway for chlorine gas (Cl_2) production[71,125]. Additionally, chlorine gas formed can undergo photolysis to regenerate chlorine atoms that can further react with organic species present[126]. Therefore, in this study, we hypothesize that the presence of chloride contributed to enhanced free radical chemistry that promoted the reactive degradation of triclosan.

Inorganic salts are also known to be one of the most hygroscopic components in aerosol particles[105]. The addition of NaCl could have increased the aerosol particle's hygroscopicity or its capacity to take up water. With increased water uptake capacity of the aerosol particles, the plasticizing effects of water could enhance diffusion and thus the probability of reaction between OH, Cl, and triclosan[105,127].

In surface water, the presence of DOM can lead to the scavenging of chlorine radicals, including chlorine atoms ($Cl^{\cdot}$) and dichlorine radical anions ($Cl_2^{\cdot -}$)[123]. Lei et al. 2020 found that

the extent of chlorine radical scavenging is largely affected by the concentration and nature of DOM present[123]. In this study, the ternary-component triclosan + NaCl + humic acid aerosol exhibited a decreased effective uptake coefficient compared to the system without humic acid but was more enhanced compared to pure triclosan (see Table 1). This phenomenon could be due to humic acid acting as an OH and chlorine radical scavenger in analogy to the discussion in Sec. 3.2.3.

In summary, the addition of NaCl contributed to an increased effective uptake coefficient/degradation rate of triclosan in the aerosol phase, which could have been facilitated by chlorine radical formation and increased diffusion in the condensed phase. The presence of humic acid, on the other hand, could have scavenged radical species and decreased the OH and chlorine radical available for heterogenous oxidation reactions with triclosan.

Chapter 3, in part, coauthored with Slade, Jonathan H., is currently being prepared for submission under the title, “Photodegradation and heterogeneous OH oxidation kinetics and products of triclosan in sea spray aerosol mimics.” The thesis author is the primary author of this chapter.

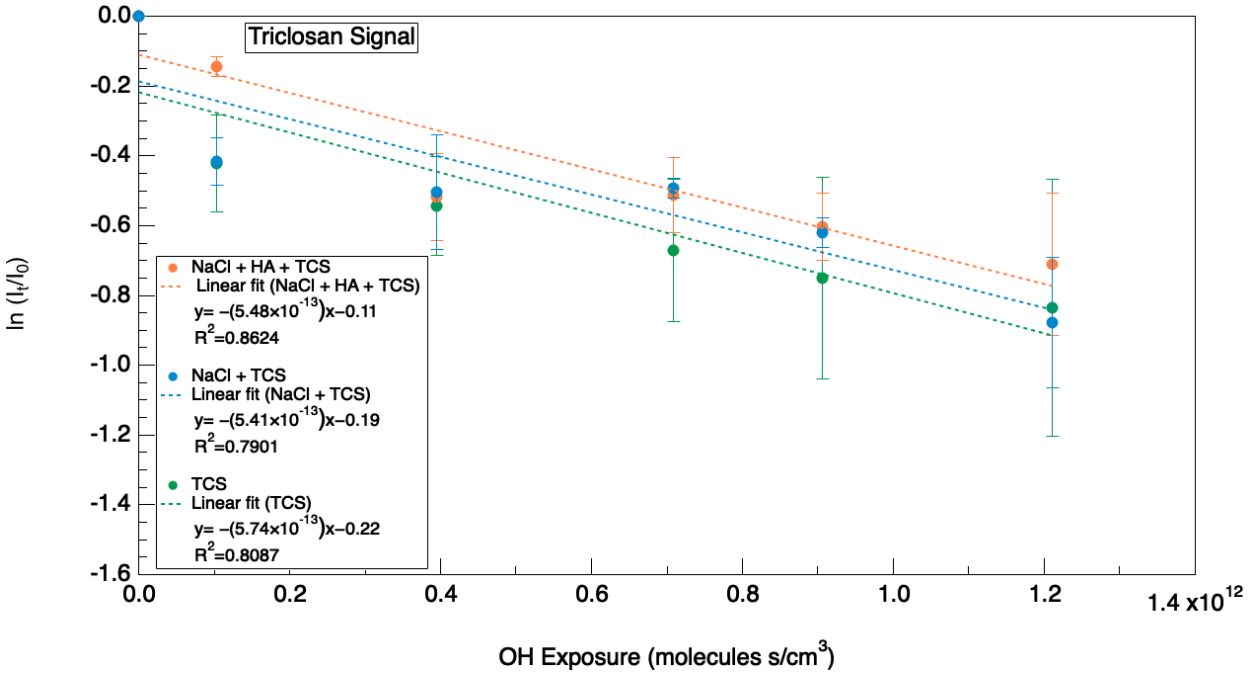

Figure 28. Triclosan degradation kinetics due to the addition of humic acid only (HA), sodium chloride only (NaCl), and both HA and NaCl as a function of OH exposure.

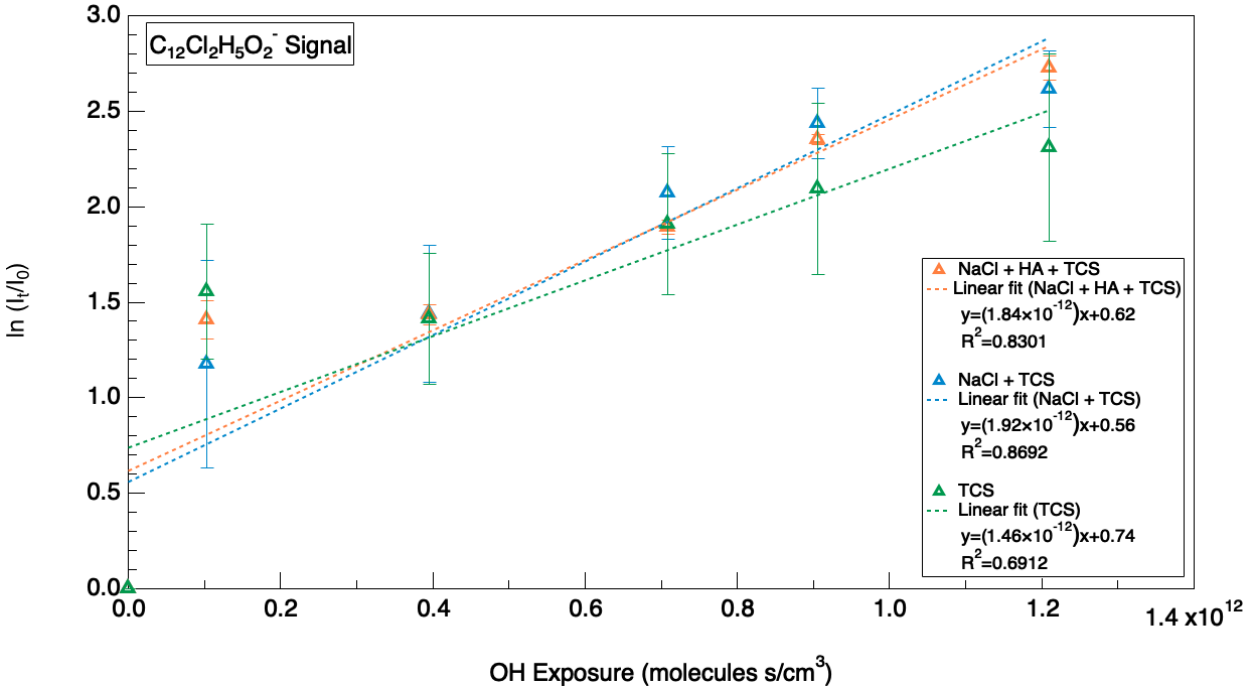

Figure 29. Photoproduct, $C_{12}Cl_2H_5O_2^-$, formation kinetics due to the addition of NaCl (NaCl + TCS), sodium chloride and humic acid (NaCl + HA + TCS) and pure-component triclosan (TCS).

Chapter Four: Conclusion and Future Work

4.1.Conclusion

The ubiquity of triclosan prompted a multitude of studies that found triclosan to induce endocrine disrupting effects in humans, are toxic to ecosystems and aquatic species, and form more toxic phototransformation products through degradation[1,19,24, 30,31,37]. Therefore, the potential for triclosan to become aerosolized in SSA from surface water and degrade in the atmosphere have important implications for human health and the environment.

The main goal of this study was to characterize triclosan photochemical degradation and heterogeneous oxidation by OH in the aerosol phase using EESI-HR-ToF-MS. The effects of CDOM and inorganic salt, which are major constituents of SSA, on triclosan photochemical degradation were also explored. Specifically, chemical aging of triclosan by OH in the aerosol phase was simulated in a PAM-OFR. Subsequent qualitative and quantitative analyses of triclosan degradation and photoproduct formation were performed using EESI-HR-ToF-MS measurements. Degradation kinetics, OH reactive uptake coefficients, and half-lives of triclosan in various particle mixtures were calculated to better understand how chemical aging by OH and light impact the environmental persistence of triclosan in particles suspended in the atmosphere.

From degradation kinetics analysis of triclosan, aerosolized triclosan was found to be photolabile and readily degraded under UV irradiance at 254nm. This characteristic is strongly attributed to the position of the chlorine substituents that can stabilize the negative charge of triclosan in its dissociated, phenolate form and promote homolytic cleavage that enables photoproduct formation through photocyclization[38,39]. On the other hand, OH heterogeneous oxidation of pure triclosan aerosol showed that triclosan degradation rates were not statistically different from that due to UV irradiance alone. Possible reasons were provided and include (1)

reduced reactivity between OH and triclosan as OH reacts with the accumulated photoproducts and oxidation products that are less reactive than triclosan at the aerosol interface and (2) slowed mass transfer of OH from the surface to the bulk driven by the potential formation of a more viscous, oxidized layer at the aerosol surface as described in previous results[110,111]. This result could be further reinforced upon photoproduct identification and analysis.

From high resolution mass spectrometry analysis and chlorine isotopic signals, photoproducts were identified according to their molecular formulae. Increase in signal intensity at the unit mass of m/z = 251 with the formula, $C_{12}Cl_2H_5O_2^-$, could have been due to the formation of DCDD, a more toxic photoproduct of triclosan[39,101,10267,101,102,105,106]. However, the identity of photoproducts observed could not be confirmed because our high-resolution mass spectrometer does not provide structural information, although there are no other expected signatures with those exact chlorine isotopes other than what can be attributed to products from triclosan photodegradation. Formation kinetics of the potential dioxin product revealed that DCDD formation is more favorable in the absence of OH and can undergo further degradation reactions to form secondary products[24,39,68]. Therefore, in this study, the photochemical degradation effects of UV irradiance appeared to dominate over the effects of OH-initiated reactions for triclosan in the aerosol phase.

The effective OH reactive uptake coefficient for pure component triclosan was 0.15 ± 0.04. However, with the addition of humic acid, a CDOM proxy, the OH reactive uptake coefficient decreased to 0.09 ± 0.04. This decrease suggests the presence of humic acid inhibits OH heterogeneous oxidization of triclosan in the aerosol phase potentially driven by OH scavenging and competitive light absorption by humic acid[112,113]. Concentration of OH available to react with triclosan particles may decrease due to competitive scavenging by humic acid as it

serves as a major sink for OH in natural waters[108,116,117]. The calculated half-lives of triclosan under the OH exposure levels explored in this study increased from 18.63 ± 4.53 days to 36.05 ± 15.25 days due to the addition of humic acid. These results indicate that the presence of humic substances in SSA may decrease the rate of triclosan heterogeneous oxidation and increase its half-life in the aerosol phase with respect to OH oxidation. However, it is important to note that our experiments were conducted in a "background" of UV irradiation at 254nm, whereas longer, less energetic wavelengths of light reach Earth's surface.

For the addition of NaCl to the triclosan system, the OH reactive uptake coefficient increased to 0.29 ± 0.08. This result points to a significant contribution of chloride-mediated heterogeneous reactions with OH to produce highly reactive chlorine gas and chlorine radicals. Chloride is a relatively large and polarizable anion, which could have undergone oxidation with OH radicals adsorbed to the aerosol surface leading to enhanced degradation of triclosan in the aerosol phase. Additionally, the presence of NaCl is expected to increase particle hygroscopicity, thereby uptake and retain more liquid water, increasing bulk diffusivity and the probability of reaction of OH and Cl with triclosan in the aerosol phase[104]. In the presence of both NaCl and humic acid, the OH reactive uptake coefficient decreased slightly to 0.24 ± 0.05, which could be attributed to the similar OH scavenging effects of CDOM mentioned previously.

Given the strong influence of UV irradiation on the degradation of triclosan in the OFR (sometimes the observed degradation was faster compared to UV irradiation + OH), the degradation of triclosan by UV irradiation alone could not reliably be subtracted to determine the uptake coefficient by OH alone. Therefore, the reported OH uptake coefficients are reported based on the observed degradation kinetics of triclosan in the presence of UV irradiation + OH. Future studies should measure OH degradation of triclosan in the dark or in presence of visible,

rather than UV radiation. Despite this consideration, the OH reactive uptake coefficient comparisons discussed in this thesis are still relevant between the different aerosol systems because the only independent variable that was altered between the different systems was the addition of humic acid, NaCl, or both. The contribution of UV irradiance to triclosan degradation was considered a consistent background present in the single-component and SSA mimic studies.

4.2 Future Work

This section details the potential for further investigation of triclosan degradation kinetics in the aerosol phase. In this study, to generate OH radicals in the PAM-OFR, UV lamps at a wavelength of 254nm were employed. Therefore, the influence of UV photolysis was present as a constant background in OH uptake kinetics analysis. To achieve environmentally relevant atmospheric oxidation conditions, future experiments can be designed to generate OH in the absence of short-wavelength UV light or radical precursors. For example, Lambe et al. 2007 have shown that atmospherically relevant OH concentrations can be sustained in chamber studies in the absence of NOx and UV light[128]. Instead, tetramethylethylene (TME) could be injected to facilitate ozonolysis reactions and generate OH in the presence of visible light[128]. Similar procedures can be followed in future lab studies to isolate the effects of OH heterogeneous oxidation of triclosan independent from the effects of UV photodegradation.

These studies involved simple single-component to ternary-component aerosol mixtures generated in the lab and consisted of equal ratios of triclosan, NaCl, and humic acid. In the natural environment, organic molecules and ions are selectively transferred from the ocean surface into SSA depending on their polarity, solubility, and lipophilicity. For more environmentally-relevant studies, it is recommended to generate the aerosol in a more

naturalistic manner, e.g., using a Marine Aerosol Reference Tank (MART) using artificial seawater and adding relevant quantities of triclosan to the surface water[129]. By inducing phytoplankton blooms, natural seawater-derived DOM could be generated instead of using humic acid as a proxy. Trueblood et al. 2019 showed distinct differences in the photosensitizing properties of natural sea water-derived DOM compared to humic and fulvic acids[130]. In addition, the effects of aerosol pH on the photosensitized degradation of triclosan were not systematically studied. Future experiments should consider systematically varying the pH of the atomizer solution using a buffer to evaluate how triclosan photodegradation rates in the aerosol phase depend on whether it is in its anionic or molecular form.

Evaluation of triclosan aerosol particle physicochemical properties is also an important concern to address. From this study, it was hypothesized that the addition of NaCl increased particle hygroscopicity, promoting greater molecular diffusivity within the particle bulk and thus a greater extent of heterogeneous reactions. Further evaluation of particle phase state (viscosity) and hygroscopicity of triclosan particles with and without NaCl and before and after heterogeneous OH oxidation can help validate this hypothesis.

Confirmation of triclosan photoproduct identity in future work may also provide insight into human health implications of triclosan photochemical degradation in the atmosphere. Offline analysis using liquid chromatopgraphy tandem mass spectrometry of aerosol filter samples and authentic standards can be used to confirm photoproduct identity. A previous cytotoxicity study on triclosan in the aqueous phase performed by Hung et al. 2018 found that a decrease in triclosan concentration did not correlate to a decrease in cytotoxicity levels. This result highlights the contribution of triclosan photoproducts to overall toxicity and, consequently, the importance of triclosan photoproduct identification and analysis.

Chapter 4, in part, coauthored with Slade, Jonathan H., is currently being prepared for submission under the title, “Photodegradation and heterogeneous OH oxidation kinetics and products of triclosan in sea spray aerosol mimics.” The thesis author is the primary author of this chapter.

References

(1) Dar, O. I.; Aslam, R.; Pan, D.; Sharma, S.; Andotra, M.; Kaur, A.; Jia, A.-Q.; Faggio, C. Source, Bioaccumulation, Degradability and Toxicity of Triclosan in Aquatic Environments: A Review. *Environ. Technol. Innov.* **2022**, *25*, 102122. https://doi.org/10.1016/j.eti.2021.102122.

(2) Dhillon, G. S.; Kaur, S.; Pulicharla, R.; Brar, S. K.; Cledón, M.; Verma, M.; Surampalli, R. Y. Triclosan: Current Status, Occurrence, Environmental Risks and Bioaccumulation Potential. *Int. J. Environ. Res. Public. Health* **2015**, *12* (5), 5657–5684. https://doi.org/10.3390/ijerph120505657.

(3) Perez, A. L.; De Sylor, M. A.; Slocombe, A. J.; Lew, M. G.; Unice, K. M.; Donovan, E. P. Triclosan Occurrence in Freshwater Systems in the United States (1999–2012): A Meta-Analysis. *Environ. Toxicol. Chem.* **2013**, *32* (7), 1479–1487. https://doi.org/10.1002/etc.2217.

(4) Yueh, M.-F.; Tukey, R. H. Triclosan: A Widespread Environmental Toxicant with Many Biological Effects. *Annu. Rev. Pharmacol. Toxicol.* **2016**, *56*, 251–272. https://doi.org/10.1146/annurev-pharmtox-010715-103417.

(5) Mohan, S.; Balakrishnan, P. Triclosan in Treated Wastewater from a City Wastewater Treatment Plant and Its Environmental Risk Assessment. *Water. Air. Soil Pollut.* **2019**, *230* (3), 69. https://doi.org/10.1007/s11270-019-4098-9.

(6) Alfhili, M. A.; Lee, M.-H. Triclosan: An Update on Biochemical and Molecular Mechanisms. *Oxid. Med. Cell. Longev.* **2019**, *2019*, e1607304. https://doi.org/10.1155/2019/1607304.

(7) Lee, D. G. Removal of a Synthetic Broad-Spectrum Antimicrobial Agent, Triclosan, in Wastewater Treatment Systems: A Short Review. *Environ. Eng. Res.* **2015**, *20* (2), 111–120. https://doi.org/10.4491/eer.2014.081.

(8) Bedoux, G.; Roig, B.; Thomas, O.; Dupont, V.; Le Bot, B. Occurrence and Toxicity of Antimicrobial Triclosan and By-Products in the Environment. *Environ. Sci. Pollut. Res. Int.* **2012**, *19* (4), 1044–1065. https://doi.org/10.1007/s11356-011-0632-z.

(9) Chen, X.; Nielsen, J. L.; Furgal, K.; Liu, Y.; Lolas, I. B.; Bester, K. Biodegradation of Triclosan and Formation of Methyl-Triclosan in Activated Sludge under Aerobic Conditions. *Chemosphere* **2011**, *84* (4), 452–456. https://doi.org/10.1016/j.chemosphere.2011.03.042.

(10) Milanović, M.; Đurić, L.; Milošević, N.; Milić, N. Comprehensive Insight into Triclosan—from Widespread Occurrence to Health Outcomes. *Environ. Sci. Pollut. Res.* **2021**. https://doi.org/10.1007/s11356-021-17273-0.

(11) Weatherly, L. M.; Gosse, J. A. Triclosan Exposure, Transformation, and Human Health Effects. *J. Toxicol. Environ. Health B Crit. Rev.* **2017**, *20* (8), 447–469. https://doi.org/10.1080/10937404.2017.1399306.

(12) Gonkowski, S.; Tzatzarakis, M.; Vakonaki, E.; Makowska, K.; Tsatsakis, A. M.; Wojtkiewicz, J. The Presence of Triclosan in Human Hair Samples in Poland—A Pilot Study. *Int. J. Environ. Res. Public. Health* **2022**, *19* (7), 3796. https://doi.org/10.3390/ijerph19073796.

(13) Safwat, N.; Abdel-Ghany, M. F.; Ayad, M. F. Sensitive Derivative Synchronous and Micellar Enhanced Ecofriendly Spectrofluorimetric Methods for the Determination of Atenolol, Diclofenac, and Triclosan in Drinking Tap Water. *J. AOAC Int.* **2021**, *104* (1), 103–112. https://doi.org/10.1093/jaoacint/qsaa100.

(14) Singer, H.; Müller, S.; Tixier, C.; Pillonel, L. Triclosan: Occurrence and Fate of a Widely Used Biocide in the Aquatic Environment: Field Measurements in Wastewater Treatment Plants, Surface Waters, and Lake Sediments. *Environ. Sci. Technol.* **2002**, *36* (23), 4998–5004. https://doi.org/10.1021/es025750i.

(15) Wang, Y.; Li, G.; Zhu, Q.; Liao, C. Occurrence of Parabens, Triclosan and Triclocarban in Paired Human Urine and Indoor Dust from Two Typical Cities in China and Its Implications for Human Exposure. *Sci. Total Environ.* **2021**, *786*, 147485. https://doi.org/10.1016/j.scitotenv.2021.147485.

(16) Chen, X.; Zhuang, J.; Bester, K. Degradation of Triclosan by Environmental Microbial Consortia and by Axenic Cultures of Microorganisms with Concerns to Wastewater Treatment. *Appl. Microbiol. Biotechnol.* **2018**, *102* (13), 5403–5417. https://doi.org/10.1007/s00253-018-9029-y.

(17) Sandborgh-Englund, G.; Adolfsson-Erici, M.; Odham, G.; Ekstrand, J. Pharmacokinetics of Triclosan Following Oral Ingestion in Humans. *J. Toxicol. Environ. Health A* **2006**, *69* (20), 1861–1873. https://doi.org/10.1080/15287390600631706.

(18) Van der Meer, T. P.; Artacho-Cordón, F.; Swaab, D. F.; Struik, D.; Makris, K. C.; Wolffenbuttel, B. H. R.; Frederiksen, H.; Van Vliet-Ostaptchouk, J. V. Distribution of Non-Persistent Endocrine Disruptors in Two Different Regions of the Human Brain. *Int. J. Environ. Res. Public. Health* **2017**, *14* (9), 1059. https://doi.org/10.3390/ijerph14091059.

(19) *Endocrine Disruptors*. National Institute of Environmental Health Sciences. https://www.niehs.nih.gov/health/topics/agents/endocrine/index.cfm (accessed 2022-08-04).

(20) Wang, X.; Chen, X.; Feng, X.; Chang, F.; Chen, M.; Xia, Y.; Chen, L. Triclosan Causes Spontaneous Abortion Accompanied by Decline of Estrogen Sulfotransferase Activity in Humans and Mice. *Sci. Rep.* **2015**, *5*, 18252. https://doi.org/10.1038/srep18252.

(21) Liu, X.; Tu, M.; Wang, S.; Wang, Y.; Wang, J.; Hou, Y.; Zheng, X.; Yan, Z. Research on Freshwater Water Quality Criteria, Sediment Quality Criteria and Ecological Risk Assessment of Triclosan in China. *Sci. Total Environ.* **2022**, *816*, 151616. https://doi.org/10.1016/j.scitotenv.2021.151616.

(22) Bakare, B. F.; Adeyinka, G. C. Occurrence and Fate of Triclosan and Triclocarban in Selected Wastewater Systems across Durban Metropolis, KwaZulu-Natal, South Africa. *Int. J. Environ. Res. Public. Health* **2022**, *19* (11), 6769. https://doi.org/10.3390/ijerph19116769.

(23) McAvoy, D. C.; Schatowitz, B.; Jacob, M.; Hauk, A.; Eckhoff, W. S. Measurement of Triclosan in Wastewater Treatment Systems. *Environ. Toxicol. Chem.* **2002**, *21* (7), 1323–1329. https://doi.org/10.1002/etc.5620210701.

(24) Mezcua, M.; Gómez, M. J.; Ferrer, I.; Aguera, A.; Hernando, M. D.; Fernández-Alba, A. R. Evidence of 2,7/2,8-Dibenzodichloro-p-Dioxin as a Photodegradation Product of Triclosan in Water and Wastewater Samples. *Anal. Chim. Acta* **2004**, *524* (1), 241–247. https://doi.org/10.1016/j.aca.2004.05.050.

(25) Bock, M.; Lyndall, J.; Barber, T.; Fuchsman, P.; Perruchon, E.; Capdevielle, M. Probabilistic Application of a Fugacity Model to Predict Triclosan Fate during Wastewater Treatment. *Integr. Environ. Assess. Manag.* **2010**, *6* (3), 393–404. https://doi.org/10.1897/IEAM_2009-070.1.

(26) Barrett, H.; Sun, J.; Gong, Y.; Yang, P.; Hao, C.; Verreault, J.; Zhang, Y.; Peng, H. Triclosan Is the Predominant Antibacterial Compound in Ontario Sewage Sludge. *Environ. Sci. Technol.* **2022**. https://doi.org/10.1021/acs.est.2c00406.

(27) van Wijnen, J.; Ragas, A. M. J.; Kroeze, C. River Export of Triclosan from Land to Sea: A Global Modelling Approach. *Sci. Total Environ.* **2018**, *621*, 1280–1288. https://doi.org/10.1016/j.scitotenv.2017.10.100.

(28) Dann, A. B.; Hontela, A. Triclosan: Environmental Exposure, Toxicity and Mechanisms of Action. *J. Appl. Toxicol.* **2011**, *31* (4), 285–311. https://doi.org/10.1002/jat.1660.

(29) Shanmugam, G.; Ramasamy, K.; Selvaraj, K. K.; Sampath, S.; Ramaswamy, B. R. Triclosan in Fresh Water Fish Gibelion Catla from the Kaveri River, India, and Its Consumption Risk Assessment. *Environ. Forensics* **2014**, *15* (3), 207–212. https://doi.org/10.1080/15275922.2014.930940.

(30) Hwang, J.; Suh, S.-S.; chang, M.; Yun Park, S.; Kwon Ryu, T.; Lee, S.; Lee, T.-K. Effects of Triclosan on Reproductive Prarmeters and Embryonic Development of Sea Urchin, Strongylocentrotus Nudus. *Ecotoxicol. Environ. Saf.* **2014**, *100*, 148–152. https://doi.org/10.1016/j.ecoenv.2013.10.029.

(31) Zhang, Y.; Liu, M.; Liu, J.; Wang, X.; Wang, C.; Ai, W.; Chen, S.; Wang, H. Combined Toxicity of Triclosan, 2,4-Dichlorophenol and 2,4,6-Trichlorophenol to Zebrafish (Danio Rerio). *Environ. Toxicol. Pharmacol.* **2018**, *57*, 9–18. https://doi.org/10.1016/j.etap.2017.11.006.

(32) Westfall, C.; Flores-Mireles, A. L.; Robinson, J. I.; Lynch, A. J. L.; Hultgren, S.; Henderson, J. P.; Levin, P. A. The Widely Used Antimicrobial Triclosan Induces High Levels of Antibiotic Tolerance In Vitro and Reduces Antibiotic Efficacy up to 100-Fold In Vivo. *Antimicrob. Agents Chemother.* **2019**, *63* (5), e02312-18. https://doi.org/10.1128/AAC.02312-18.

(33) *Safety and Effectiveness of Consumer Antiseptics; Topical Antimicrobial Drug Products for Over-the-Counter Human Use*. Federal Register. https://www.federalregister.gov/documents/2016/09/06/2016-21337/safety-and-effectiveness-of-consumer-antiseptics-topical-antimicrobial-drug-products-for (accessed 2022-08-02).

(34) Canada, H. *Triclosan*. https://www.canada.ca/en/health-canada/services/chemicals-product-safety/triclosan.html (accessed 2022-08-01).

(35) *Safety of Triclocarban and Triclosan as substances with potential endocrine disrupting properties in cosmetic products*. https://health.ec.europa.eu/publications/safety-triclocarban-and-triclosan-substances-potential-endocrine-disrupting-properties-cosmetic_en (accessed 2022-08-05).

(36) Chen, Y.; Fang, J.; Ren, L.; Fan, R.; Zhang, J.; Liu, G.; Zhou, L.; Chen, D.; Yu, Y.; Lu, S. Urinary Bisphenol Analogues and Triclosan in Children from South China and Implications for Human Exposure. *Environ. Pollut.* **2018**, *238*, 299–305. https://doi.org/10.1016/j.envpol.2018.03.031.

(37) Iovino, P.; Chianese, S.; Prisciandaro, M.; Musmarra, D. Triclosan Photolysis: Operating Condition Study and Photo-Oxidation Pathway. *Chem. Eng. J.* **2019**, *377*, 121045. https://doi.org/10.1016/j.cej.2019.02.132.

(38) Solá-Gutiérrez, C.; Schröder, S.; San-Román, M. F.; Ortiz, I. Critical Review on the Mechanistic Photolytic and Photocatalytic Degradation of Triclosan. *J. Environ. Manage.* **2020**, *260*, 110101. https://doi.org/10.1016/j.jenvman.2020.110101.

(39) Apell, J. N.; Kliegman, S.; Solá-Gutiérrez, C.; McNeill, K. Linking Triclosan's Structural Features to Its Environmental Fate and Photoproducts. *Environ. Sci. Technol.* **2020**, *54* (22), 14432–14441. https://doi.org/10.1021/acs.est.0c05121.

(40) *United Nations Treaty Collection*. https://treaties.un.org/Pages/ViewDetails.aspx?src=IND&mtdsg_no=XXVII-15&chapter=27&clang=_en (accessed 2022-08-09).

(41) Bukowska, B.; Wieteska, P.; Kwiatkowska, M.; Sicińska, P.; Michalowicz, J. Evaluation of the Effect of 2,4-Dichlorophenol on Oxidative Parameters and Viability of Human Blood Mononuclear Cells (in Vitro). *Hum. Exp. Toxicol.* **2016**, *35* (7), 775–784. https://doi.org/10.1177/0960327115606789.

(42) Gong, S. L.; Barrie, L. A.; Lazare, M. Canadian Aerosol Module (CAM): A Size-Segregated Simulation of Atmospheric Aerosol Processes for Climate and Air Quality Models 2. Global Sea-Salt Aerosol and Its Budgets. *J. Geophys. Res. Atmospheres* **2002**, *107* (D24), AAC 13-1-AAC 13-14. https://doi.org/10.1029/2001JD002004.

(43) Cochran, R. E.; Jayarathne, T.; Stone, E. A.; Grassian, V. H. Selectivity Across the Interface: A Test of Surface Activity in the Composition of Organic-Enriched Aerosols from Bubble Bursting. *J. Phys. Chem. Lett.* **2016**, *7* (9), 1692–1696. https://doi.org/10.1021/acs.jpclett.6b00489.

(44) Luo, M. Structure, Properties, Dynamics, and Photochemical Behavior of Organic and Biological Species in Marine-Relevant Environments, UC San Diego, 2021. https://escholarship.org/uc/item/5ns1h9hv (accessed 2022-08-10).

(45) Cochran, R. E.; Ryder, O. S.; Grassian, V. H.; Prather, K. A. Sea Spray Aerosol: The Chemical Link between the Oceans, Atmosphere, and Climate. *Acc. Chem. Res.* **2017**, *50* (3), 599–604. https://doi.org/10.1021/acs.accounts.6b00603.

(46) Richard, C.; Canonica, S. Aquatic Phototransformation of Organic Contaminants Induced by ColouredDissolved Natural Organic Matter. In *Environmental Photochemistry Part II*; Boule, P., Bahnemann, D. W., Robertson, P. K. J., Eds.; The Handbook of Environmental Chemistry; Springer: Berlin, Heidelberg, 2005; pp 299–323. https://doi.org/10.1007/b138187.

(47) Vione, D.; Scozzaro, A. Photochemistry of Surface Fresh Waters in the Framework of Climate Change. *Environ. Sci. Technol.* **2019**, *53* (14), 7945–7963. https://doi.org/10.1021/acs.est.9b00968.

(48) Frimmel, F. H. Photochemical Aspects Related to Humic Substances. *Environ. Int.* **1994**, *20* (3), 373–385. https://doi.org/10.1016/0160-4120(94)90123-6.

(49) Chen, L.; Wang, Z.; Wang, Z.; Gu, X. Influence of Humic Acid on the Photolysis of Triclosan in Different Dissociation Forms. *Water. Air. Soil Pollut.* **2016**, *227* (9), 318. https://doi.org/10.1007/s11270-016-3024-7.

(50) Ciuraru, R.; Fine, L.; van Pinxteren, M.; D'Anna, B.; Herrmann, H.; George, C. Photosensitized Production of Functionalized and Unsaturated Organic Compounds at the Air-Sea Interface. *Sci. Rep.* **2015**, *5* (1), 12741. https://doi.org/10.1038/srep12741.

(51) Collins, D. B.; Zhao, D. F.; Ruppel, M. J.; Laskina, O.; Grandquist, J. R.; Modini, R. L.; Stokes, M. D.; Russell, L. M.; Bertram, T. H.; Grassian, V. H.; Deane, G. B.; Prather, K.

A. Direct Aerosol Chemical Composition Measurements to Evaluate the Physicochemical Differences between Controlled Sea Spray Aerosol Generation Schemes. *Atmospheric Meas. Tech.* **2014**, *7* (11), 3667–3683. https://doi.org/10.5194/amt-7-3667-2014.

(52) Grythe, H.; Ström, J.; Krejci, R.; Quinn, P.; Stohl, A. A Review of Sea-Spray Aerosol Source Functions Using a Large Global Set of Sea Salt Aerosol Concentration Measurements. *Atmospheric Chem. Phys.* **2014**, *14* (3), 1277–1297. https://doi.org/10.5194/acp-14-1277-2014.

(53) Luo, M.; Shemesh, D.; Sullivan, M. N.; Alves, M. R.; Song, M.; Gerber, R. B.; Grassian, V. H. Impact of PH and NaCl and CaCl2 Salts on the Speciation and Photochemistry of Pyruvic Acid in the Aqueous Phase. *J. Phys. Chem. A* **2020**, *124* (25), 5071–5080. https://doi.org/10.1021/acs.jpca.0c01016.

(54) Gao, Y.; Yan, M.; Korshin, G. V. Effects of Ionic Strength on the Chromophores of Dissolved Organic Matter. *Environ. Sci. Technol.* **2015**, *49* (10), 5905–5912. https://doi.org/10.1021/acs.est.5b00601.

(55) Riedel, K.; Lassey, K. Detergent of the Atmosphere. *Water Atmos* **2008**, *16*.

(56) Li, M.; Karu, E.; Brenninkmeijer, C.; Fischer, H.; Lelieveld, J.; Williams, J. Tropospheric OH and Stratospheric OH and Cl Concentrations Determined from CH4, CH3Cl, and SF6 Measurements. *Npj Clim. Atmospheric Sci.* **2018**, *1* (1), 1–7. https://doi.org/10.1038/s41612-018-0041-9.

(57) *Abstract - Paul Crutzen (2002)*. Lindau Nobel Mediatheque. https://www.mediatheque.lindau-nobel.org/abstracts/30485/2002-the-importance-of-the-tropics-in-atmospheric-chemistry-and-climate/laureate-crutzen (accessed 2022-08-09).

(58) *Environmental Chemistry, 5th Edition | Macmillan Learning for Instructors*. https://www.macmillanlearning.com/college/us/product/Environmental-Chemistry/p/1429277041?selected_tab=Contents (accessed 2022-08-09).

(59) *7.4.5 The Hydroxyl Radical - AR4 WGI Chapter 7: Couplings Between Changes in the Climate System and Biogeochemistry*. https://archive.ipcc.ch/publications_and_data/ar4/wg1/en/ch7s7-4-5.html (accessed 2022-08-09).

(60) Lelieveld, J.; Gromov, S.; Pozzer, A.; Taraborrelli, D. Global Tropospheric Hydroxyl Distribution, Budget and Reactivity. *Atmospheric Chem. Phys.* **2016**, *16* (19), 12477–12493. https://doi.org/10.5194/acp-16-12477-2016.

(61) Ma, J.; Zhu, C.; Lu, J.; Lei, Y.; Wang, J.; Chen, T. Photochemical Reaction between Triclosan and Nitrous Acid in the Atmospheric Aqueous Environment. *Atmos. Environ.* **2017**, *157*, 38–48. https://doi.org/10.1016/j.atmosenv.2017.03.011.

(62) Kleffmann, J. Daytime Sources of Nitrous Acid (HONO) in the Atmospheric Boundary Layer. *ChemPhysChem* **2007**, *8* (8), 1137–1144. https://doi.org/10.1002/cphc.200700016.

(63) Li, L.; Duan, Z.; Li, H.; Zhu, C.; Henkelman, G.; Francisco, J. S.; Zeng, X. C. Formation of HONO from the NH3-Promoted Hydrolysis of NO2 Dimers in the Atmosphere. *Proc. Natl. Acad. Sci.* **2018**, *115* (28), 7236–7241. https://doi.org/10.1073/pnas.1807719115.

(64) Akimoto, H.; Hirokawa, J. Atmospheric Multiphase Chemistry. **2020**.

(65) Slade, J. H.; Knopf, D. A. Multiphase OH Oxidation Kinetics of Organic Aerosol: The Role of Particle Phase State and Relative Humidity. *Geophys. Res. Lett.* **2014**, *41* (14), 5297–5306. https://doi.org/10.1002/2014GL060582.

(66) Slade, J. H.; Knopf, D. A. Heterogeneous OH Oxidation of Biomass Burning Organic Aerosol Surrogate Compounds: Assessment of Volatilisation Products and the Role of OH Concentration on the Reactive Uptake Kinetics. *Phys. Chem. Chem. Phys.* **2013**, *15* (16), 5898–5915. https://doi.org/10.1039/C3CP44695F.

(67) Sanchez-Prado, L.; Llompart, M.; Lores, M.; García-Jares, C.; Bayona, J. M.; Cela, R. Monitoring the Photochemical Degradation of Triclosan in Wastewater by UV Light and Sunlight Using Solid-Phase Microextraction. *Chemosphere* **2006**, *65* (8), 1338–1347. https://doi.org/10.1016/j.chemosphere.2006.04.025.

(68) Latch, D. E.; Packer, J. L.; Stender, B. L.; VanOverbeke, J.; Arnold, W. A.; McNeill, K. Aqueous Photochemistry of Triclosan: Formation of 2,4-Dichlorophenol, 2,8-Dichlorodibenzo-p-Dioxin, and Oligomerization Products. *Environ. Toxicol. Chem.* **2005**, *24* (3), 517–525. https://doi.org/10.1897/04-243R.1.

(69) Tixier, C.; Singer, H. P.; Canonica, S.; Müller, S. R. Phototransformation of Triclosan in Surface Waters: A Relevant Elimination Process for This Widely Used BiocideLaboratory Studies, Field Measurements, and Modeling. *Environ. Sci. Technol.* **2002**, *36* (16), 3482–3489. https://doi.org/10.1021/es025647t.

(70) Chen, L.; Wang, Z.; Qian, C.; He, Y. *Effects of inorganic anions on the photolysis of triclosan under UV irradiation | Water Science & Technology | IWA Publishing*. https://iwaponline.com/wst/article/78/7/1476/64149/Effects-of-inorganic-anions-on-the-photolysis-of (accessed 2022-08-23).

(71) Knipping, E. M.; Lakin, M. J.; Foster, K. L.; Jungwirth, P.; Tobias, D. J.; Gerber, R. B.; Dabdub, D.; Finlayson-Pitts, B. J. Experiments and Simulations of Ion-Enhanced Interfacial Chemistry on Aqueous NaCl Aerosols. *Science* **2000**, *288* (5464), 301–306. https://doi.org/10.1126/science.288.5464.301.

(72) Aranami, K.; Readman, J. W. Photolytic Degradation of Triclosan in Freshwater and Seawater. *Chemosphere* **2007**, *66* (6), 1052–1056. https://doi.org/10.1016/j.chemosphere.2006.07.010.

(73) *Major Ions in Seawater - Angelis - Major Reference Works - Wiley Online Library*. https://onlinelibrary.wiley.com/doi/full/10.1002/047147844X.oc1707 (accessed 2022-08-23).

(74) Liu, B. Y.; Lee, K. W. An Aerosol Generator of High Stability. *Am. Ind. Hyg. Assoc. J.* **1975**, *36* (12), 861–865. https://doi.org/10.1080/0002889758507357.

(75) Model 3076 Constant Output Atomizer Instruction Manual. 63.

(76) Brechtel Instrument Manaul SEMS 2100, 2021. https://www.brechtel.com/wp-content/uploads/2021/08/bmi_model_2100_SEMS_manual_v3.1.pdf.

(77) Sorooshian, A.; Hersey, S.; Brechtel, F. J.; Corless, A.; Flagan, R. C.; Seinfeld, J. H. Rapid, Size-Resolved Aerosol Hygroscopic Growth Measurements: Differential Aerosol Sizing and Hygroscopicity Spectrometer Probe (DASH-SP). *Aerosol Sci. Technol.* **2008**, *42* (6), 445–464. https://doi.org/10.1080/02786820802178506.

(78) Knutson, E. O.; Whitby, K. T. Aerosol Classification by Electric Mobility: Apparatus, Theory, and Applications. *J. Aerosol Sci.* **1975**, *6* (6), 443–451. https://doi.org/10.1016/0021-8502(75)90060-9.

(79) Model 1720 Mixing Condensation Particle Counter Manual, 2016.

(80) Kang, E.; Root, M. J.; Toohey, D. W.; Brune, W. H. Introducing the Concept of Potential Aerosol Mass (PAM). *Atmospheric Chem. Phys.* **2007**, *7* (22), 5727–5744. https://doi.org/10.5194/acp-7-5727-2007.

(81) Lambe, A. T.; Ahern, A. T.; Williams, L. R.; Slowik, J. G.; Wong, J. P. S.; Abbatt, J. P. D.; Brune, W. H.; Ng, N. L.; Wright, J. P.; Croasdale, D. R.; Worsnop, D. R.; Davidovits, P.; Onasch, T. B. Characterization of Aerosol Photooxidation Flow Reactors: Heterogeneous Oxidation, Secondary Organic Aerosol Formation and Cloud Condensation Nuclei Activity Measurements. *Atmospheric Meas. Tech.* **2011**, *4* (3), 445–461. https://doi.org/10.5194/amt-4-445-2011.

(82) Li, R.; Palm, B. B.; Ortega, A. M.; Hlywiak, J.; Hu, W.; Peng, Z.; Day, D. A.; Knote, C.; Brune, W. H.; de Gouw, J. A.; Jimenez, J. L. Modeling the Radical Chemistry in an Oxidation Flow Reactor: Radical Formation and Recycling, Sensitivities, and the OH Exposure Estimation Equation. *J. Phys. Chem. A* **2015**, *119* (19), 4418–4432. https://doi.org/10.1021/jp509534k.

(83) Rowe, J.; Lambe, A.; Brune, W. *ACP - Technical Note: Effect of varying the λ = 185 and 254 nm photon flux ratio on radical generation in oxidation flow reactors*. https://acp.copernicus.org/articles/20/13417/2020/ (accessed 2022-08-18).

(84) Mayer, K. J. Secondary Marine Aerosol: A Chemical Link Between Oceans and Clouds, UC San Diego, La Jolla, 2021. https://escholarship.org/uc/item/75q3629h.

(85) Chen, W.-C.; Marcus, R. A. On the Theory of the Reaction Rate of Vibrationally Excited CO Molecules with OH Radicals. *J. Chem. Phys.* **2005**, *124* (2).

(86) Seinfeld, J. H.; Pandis, S. N. *ATMOSPHERIC CHEMISTRY AND PHYSICS From Air Pollution to Climate Change*, Second.; John Wiley & Sons, Inc.: New Jersey, 2006.

(87) Ozone Monitor Operation Manual - Models 106-M and 106-OEM-M, 2018.

(88) Lopez-Hilfiker, F. D.; Pospisilova, V.; Huang, W.; Kalberer, M.; Mohr, C.; Stefenelli, G.; Thornton, J. A.; Baltensperger, U.; Prevot, A. S. H.; Slowik, J. G. An Extractive Electrospray Ionization Time-of-Flight Mass Spectrometer (EESI-TOF) for Online Measurement of Atmospheric Aerosol Particles. *Atmospheric Meas. Tech.* **2019**, *12* (9), 4867–4886. https://doi.org/10.5194/amt-12-4867-2019.

(89) Chen, H.; Venter, A.; Cooks, R. G. Extractive Electrospray Ionization for Direct Analysis of Undiluted Urine, Milk and Other Complex Mixtures without Sample Preparation. *Chem. Commun.* **2006**, No. 19, 2042–2044. https://doi.org/10.1039/B602614A.

(90) Wang, R.; Gröhn, A. J.; Zhu, L.; Dietiker, R.; Wegner, K.; Günther, D.; Zenobi, R. On the Mechanism of Extractive Electrospray Ionization (EESI) in the Dual-Spray Configuration. *Anal. Bioanal. Chem.* **2012**, *402* (8), 2633–2643. https://doi.org/10.1007/s00216-011-5471-8.

(91) Pospisilova, V.; Lopez-Hilfiker, F. D.; Bell, D. M.; Haddad, I. E.; Mohr, C.; Huang, W.; Heikkinen, L.; Xiao, M.; Dommen, J.; Prevot, A. S. H.; Baltensperger, U.; Slowik, J. G. *On the fate of oxygenated organic molecules in atmospheric aerosol particles | Science Advances*. https://www.science.org/doi/10.1126/sciadv.aax8922 (accessed 2022-08-23).

(92) Pagonis, D.; Campuzano-Jost, P.; Guo, H.; Day, D. A.; Schueneman, M. K.; Brown, W. L.; Nault, B. A.; Stark, H.; Siemens, K.; Laskin, A.; Piel, F.; Tomsche, L.; Wisthaler, A.; Coggon, M. M.; Gkatzelis, G. I.; Halliday, H. S.; Krechmer, J. E.; Moore, R. H.; Thomson, D. S.; Warneke, C.; Wiggins, E. B.; Jimenez, J. L. Airborne Extractive Electrospray Mass Spectrometry Measurements of the Chemical Composition of Organic Aerosol. *Atmospheric Meas. Tech.* **2021**, *14* (2), 1545–1559. https://doi.org/10.5194/amt-14-1545-2021.

(93) Kruve, A.; Kaupmees, K.; Liigand, J.; Leito, I. Negative Electrospray Ionization via Deprotonation: Predicting the Ionization Efficiency. *Anal. Chem.* **2014**, *86* (10), 4822–4830. https://doi.org/10.1021/ac404066v.

(94) Gallimore, P. J.; Kalberer, M. Characterizing an Extractive Electrospray Ionization (EESI) Source for the Online Mass Spectrometry Analysis of Organic Aerosols. *Environ. Sci. Technol.* **2013**, *47* (13), 7324–7331. https://doi.org/10.1021/es305199h.

(95) Kulkarni, P.; Baron, P. A.; Willeke, K. *Aerosol Measurement Principles, Techniques, and Applications*, Third.; John Wiley & Sons, Inc.: New Jersey, 2011.

(96) Zhang, Y.; Liu, P.; Han, Y.; Li, Y.; Chen, Q.; Kuwata, M.; Martin, S. T. *Aerosols in Atmospheric Chemistry*. ACS Publications. https://doi.org/10.1021/acsinfocus.7e5020.

(97) George, I. J.; Abbatt, J. P. D. Heterogeneous Oxidation of Atmospheric Aerosol Particles by Gas-Phase Radicals. *Nat. Chem.* **2010**, *2* (9), 713–722. https://doi.org/10.1038/nchem.806.

(98) Tang, M. J.; Shiraiwa, M.; Pöschl, U.; Cox, R. A.; Kalberer, M. Compilation and Evaluation of Gas Phase Diffusion Coefficients of Reactive Trace Gases in the Atmosphere: Volume 2. Diffusivities of Organic Compounds, Pressure-Normalised Mean Free Paths, and Average Knudsen Numbers for Gas Uptake Calculations. *Atmospheric Chem. Phys.* **2015**, *15* (10), 5585–5598. https://doi.org/10.5194/acp-15-5585-2015.

(99) Kessler, S. H.; Smith, J. D.; Che, D. L.; Worsnop, D. R.; Wilson, K. R.; Kroll, J. H. Chemical Sinks of Organic Aerosol: Kinetics and Products of the Heterogeneous Oxidation of Erythritol and Levoglucosan. *Environ. Sci. Technol.* **2010**, *44* (18), 7005–7010. https://doi.org/10.1021/es101465m.

(100) Wagner, C.; Hanisch, F.; Holmes, N.; de Coninck, H.; Schuster, G.; Crowley, J. N. The Interaction of N_2O_5 with Mineral Dust: Aerosol Flow Tube and Knudsen Reactor Studies. *Atmospheric Chem. Phys.* **2008**, *8* (1), 91–109. https://doi.org/10.5194/acp-8-91-2008.

(101) Wong-Wah-Chung, P.; Rafqah, S.; Voyard, G.; Sarakha, M. Photochemical Behaviour of Triclosan in Aqueous Solutions: Kinetic and Analytical Studies. *J. Photochem. Photobiol. Chem.* **2007**, *191* (2), 201–208. https://doi.org/10.1016/j.jphotochem.2007.04.024.

(102) Kliegman, S.; Eustis, S. N.; Arnold, W. A.; McNeill, K. Experimental and Theoretical Insights into the Involvement of Radicals in Triclosan Phototransformation. *Environ. Sci. Technol.* **2013**, *47* (13), 6756–6763. https://doi.org/10.1021/es3041797.

(103) Lee, C. P.; Surdu, M.; Bell, D. M.; Lamkaddam, H.; Wang, M.; Ataei, F.; Hofbauer, V.; Lopez, B.; Donahue, N. M.; Dommen, J.; Prevot, A. S. H.; Slowik, J. G.; Wang, D.; Baltensperger, U.; El Haddad, I. Effects of Aerosol Size and Coating Thickness on the Molecular Detection Using Extractive Electrospray Ionization. *Atmospheric Meas. Tech.* **2021**, *14* (9), 5913–5923. https://doi.org/10.5194/amt-14-5913-2021.

(104) Verma, V.; Pakbin, P.; Cheung, K. L.; Cho, A. K.; Schauer, J. J.; Shafer, M. M.; Kleinman, M. T.; Sioutas, C. Physicochemical and Oxidative Characteristics of Semi-Volatile Components of Quasi-Ultrafine Particles in an Urban Atmosphere. *Atmos. Environ.* **2011**, *45* (4), 1025–1033. https://doi.org/10.1016/j.atmosenv.2010.10.044.

(105) Davies, J. F.; Wilson, K. R. Chapter 13 - Heterogeneous Reactions in Aerosol. In *Physical Chemistry of Gas-Liquid Interfaces*; Faust, J. A., House, J. E., Eds.; Developments in Physical & Theoretical Chemistry; Elsevier, 2018; pp 403–433. https://doi.org/10.1016/B978-0-12-813641-6.00013-3.

(106) Zhang, X.; Zhang, C.; Sun, X.; Kang, L.; Zhao, Y. Chemical Conversion Pathways and Kinetic Modeling for the OH-Initiated Reaction of Triclosan in Gas-Phase. *Int. J. Mol. Sci.* **2015**, *16* (4), 8128–8141. https://doi.org/10.3390/ijms16048128.

(107) Gao, Y.; Ji, Y.; Li, G.; An, T. Mechanism, Kinetics and Toxicity Assessment of OH-Initiated Transformation of Triclosan in Aquatic Environments. *Water Res.* **2014**, *49*, 360–370. https://doi.org/10.1016/j.watres.2013.10.027.

(108) da Luz, V. C.; Bazoti, S. F.; Behling, L.; Dalla Rosa, C.; Pasquali, G. D. L. Enhanced UV Direct Photolysis and UV/H2O2 for Oxidation of Triclosan and Ibuprofen in Synthetic Effluent: An Experimental Study. *Water. Air. Soil Pollut.* **2022**, *233* (4), 126. https://doi.org/10.1007/s11270-022-05583-z.

(109) Bianco, A.; Fabbri, D.; Minella, M.; Brigante, M.; Mailhot, G.; Maurino, V.; Minero, C.; Vione, D. New Insights into the Environmental Photochemistry of 5-Chloro-2-(2,4-Dichlorophenoxy)Phenol (Triclosan): Reconsidering the Importance of Indirect Photoreactions. *Water Res.* **2015**, *72*, 271–280. https://doi.org/10.1016/j.watres.2014.07.036.

(110) Arangio, A. M.; Slade, J. H.; Berkemeier, T.; Pöschl, U.; Knopf, D. A.; Shiraiwa, M. Multiphase Chemical Kinetics of OH Radical Uptake by Molecular Organic Markers of Biomass Burning Aerosols: Humidity and Temperature Dependence, Surface Reaction, and Bulk Diffusion. *J. Phys. Chem. A* **2015**, *119* (19), 4533–4544. https://doi.org/10.1021/jp510489z.

(111) Hosny, N. A.; Fitzgerald, C.; Vyšniauskas, A.; Athanasiadis, A.; Berkemeier, T.; Uygur, N.; Pöschl, U.; Shiraiwa, M.; Kalberer, M.; Pope, F. D.; Kuimova, M. K. Direct Imaging of Changes in Aerosol Particle Viscosity upon Hydration and Chemical Aging. *Chem. Sci.* **2016**, *7* (2), 1357–1367. https://doi.org/10.1039/C5SC02959G.

(112) Munoz, M.; de Pedro, Z. M.; Casas, J. A.; Rodriguez, J. J. Triclosan Breakdown by Fenton-like Oxidation. *Chem. Eng. J.* **2012**, *198–199*, 275–281. https://doi.org/10.1016/j.cej.2012.05.097.

(113) Boule, P.; Guyon, C.; Lemaire, J. Photochemistry and Environment IV- Photochemical Behaviour of Monochlorophenols in Dilute Aqueous Solution. *Chemosphere* **1982**, *11* (12), 1179–1188. https://doi.org/10.1016/0045-6535(82)90031-5.

(114) Finlayson-Pitts, B. J.; Pitts, J. N. CHAPTER 5 - Kinetics and Atmospheric Chemistry. In *Chemistry of the Upper and Lower Atmosphere*; Finlayson-Pitts, B. J., Pitts, J. N., Eds.; Academic Press: San Diego, 2000; pp 130–178. https://doi.org/10.1016/B978-012257060-5/50007-1.

(115) Chen, Y.; Liu, L.; Su, J.; Liang, J.; Wu, B.; Zuo, J.; Zuo, Y. Role of Humic Substances in the Photodegradation of Naproxen under Simulated Sunlight. *Chemosphere* **2017**, *187*, 261–267. https://doi.org/10.1016/j.chemosphere.2017.08.110.

(116) Wenk, J.; von Gunten, U.; Canonica, S. Effect of Dissolved Organic Matter on the Transformation of Contaminants Induced by Excited Triplet States and the Hydroxyl Radical. *Environ. Sci. Technol.* **2011**, *45* (4), 1334–1340. https://doi.org/10.1021/es102212t.

(117) Chen, L.; Tang, X.; Shen, C.; Chen, C.; Chen, Y. Photosensitized Degradation of 2,4′,5-Trichlorobiphenyl (PCB 31) by Dissolved Organic Matter. *J. Hazard. Mater.* **2012**, *201–202*, 1–6. https://doi.org/10.1016/j.jhazmat.2011.10.061.

(118) Ozaki, N.; Tanaka, T.; Kindaichi, T.; Ohashi, A. Photodegradation of Fragrance Materials and Triclosan in Water: Direct Photolysis and Photosensitized Degradation. *Environ. Technol. Innov.* **2021**, *23*, 101766. https://doi.org/10.1016/j.eti.2021.101766.

(119) Brezonik, P. L.; Fulkerson-Brekken, J. Nitrate-Induced Photolysis in Natural Waters: Controls on Concentrations of Hydroxyl Radical Photo-Intermediates by Natural Scavenging Agents. *Environ. Sci. Technol.* **1998**, *32* (19), 3004–3010. https://doi.org/10.1021/es9802908.

(120) Goldstone, J. V.; Pullin, M. J.; Bertilsson, S.; Voelker, B. M. Reactions of Hydroxyl Radical with Humic Substances: Bleaching, Mineralization, and Production of Bioavailable Carbon Substrates. *Environ. Sci. Technol.* **2002**, *36* (3), 364–372. https://doi.org/10.1021/es0109646.

(121) Huang, Y.; Liu, Y.; Kong, M.; Xu, E. G.; Coffin, S.; Schlenk, D.; Dionysiou, D. D. Efficient Degradation of Cytotoxic Contaminants of Emerging Concern by UV/H2O2. *Environ. Sci. Water Res. Technol.* **2018**, *4* (9), 1272–1281. https://doi.org/10.1039/C8EW00290H.

(122) Zhang, K.; Parker, K. M. Halogen Radical Oxidants in Natural and Engineered Aquatic Systems. *Environ. Sci. Technol.* **2018**, *52* (17), 9579–9594. https://doi.org/10.1021/acs.est.8b02219.

(123) Lei, Y.; Lei, X.; Westerhoff, P.; Zhang, X.; Yang, X. Reactivity of Chlorine Radicals (Cl• and Cl2•–) with Dissolved Organic Matter and the Formation of Chlorinated Byproducts. *Environ. Sci. Technol.* **2021**, *55* (1), 689–699. https://doi.org/10.1021/acs.est.0c05596.

(124) Roeselová, M.; Jungwirth, P.; Tobias, D. J.; Gerber, R. B. Impact, Trapping, and Accommodation of Hydroxyl Radical and Ozone at Aqueous Salt Aerosol Surfaces. A Molecular Dynamics Study. *J. Phys. Chem. B* **2003**, *107* (46), 12690–12699. https://doi.org/10.1021/jp030592i.

(125) Thomas, J. L.; Jimenez-Aranda, A.; Finlayson-Pitts, B. J.; Dabdub, D. Gas-Phase Molecular Halogen Formation from NaCl and NaBr Aerosols: When Are Interface Reactions Important? *J. Phys. Chem. A* **2006**, *110* (5), 1859–1867. https://doi.org/10.1021/jp054911c.

(126) Oum, K. W.; Lakin, M. J.; DeHaan, D. O.; Brauers, T.; Finlayson-Pitts, B. J. Formation of Molecular Chlorine from the Photolysis of Ozone and Aqueous Sea-Salt Particles. *Science* **1998**, *279* (5347), 74–76. https://doi.org/10.1126/science.279.5347.74.

(127) Mikhailov, E.; Vlasenko, S.; Martin, S. T.; Koop, T.; Pöschl, U. Amorphous and Crystalline Aerosol Particles Interacting with Water Vapor: Conceptual Framework and Experimental Evidence for Restructuring, Phase Transitions and Kinetic Limitations. *Atmospheric Chem. Phys.* **2009**, *9* (24), 9491–9522. https://doi.org/10.5194/acp-9-9491-2009.

(128) Lambe, A. T.; Zhang, J.; Sage, A. M.; Donahue, N. M. Controlled OH Radical Production via Ozone-Alkene Reactions for Use in Aerosol Aging Studies. *Environ. Sci. Technol.* **2007**, *41* (7), 2357–2363. https://doi.org/10.1021/es061878e.

(129) Stokes, M. D.; Deane, G. B.; Prather, K.; Bertram, T. H.; Ruppel, M. J.; Ryder, O. S.; Brady, J. M.; Zhao, D. A Marine Aerosol Reference Tank System as a Breaking Wave Analogue for the Production of Foam and Sea-Spray Aerosols. *Atmospheric Meas. Tech.* **2013**, *6* (4), 1085–1094. https://doi.org/10.5194/amt-6-1085-2013.

(130) Trueblood, J. V.; Alves, M. R.; Power, D.; Santander, M. V.; Cochran, R. E.; Prather, K. A.; Grassian, V. H. Shedding Light on Photosensitized Reactions within Marine-Relevant Organic Thin Films. *ACS Earth Space Chem.* **2019**, *3* (8), 1614–1623. https://doi.org/10.1021/acsearthspacechem.9b00066.